GLASS LASER RESEARCH

R.D. Maurer, et al.

Corning Glass Works
Corning, New York

15 August 1965

Glass Laser Research

SEMIANNUAL REPORT for
Office of Naval Research
Contract No. Nonr-3C 33(00)

JULY 1965

CORNING
CORNING GLASS WORKS

SEMIANNUAL TECHNICAL REPORT

December 1964 to July 15, 1965

Contract Nonr - 3833(00)

August 15, 1965

Glass Laser Research

Corning Glass Works

Corning, New York

Order No. 306-62

Project Code No. 7300

Authors: CGW

R. D. Maurer

M. E. Vance

G. E. Stong

N. F. Borrelli

TRG

S. D. Sims

J. E. Dennis

This research is a part of Project DEFENDER under the joint sponsorship of the Advanced Research Projects Agency, the Office of Naval Research, and the Department of Defense.

ABSTRACT

This report presents additional data on the properties of glass used in lasers as well as operating characteristics of glass lasers. The effect of intense ultraviolet radiation is shown to decrease the output of glass lasers much more than can be accounted for the decrease in fluorescence intensity or absorption of pump light. Comprehensive threshold and output data are given for several lasers of Code 0580 glass. These data can be approximately described by the theory of Miles and Goldstein using an internal oscillator loss only slightly higher than the measured static loss in the glass. Gain data of a glass laser amplifier show the difference between a glass laser probe and a narrow band probe with respect to averaging over the fluorescence line. Finally, quantitative measurements of the birefrigence following pumping are given.

TABLE OF CONTENTS

INTRODUCTION

The following is a delayed report which gives the remaining work completed on this phase of the contract. The past year, Corning Glass Works subcontracted TRG, a subsidiary of Control Data, and the two groups carried out a cooperative effort. Each company provided approximately one half the total effort. The section headings below are followed by an identification in parentheses which tells where the work was performed. Corning Glass Works has supplied primarily glass research and TRG has measured some of the properties needed to properly design devices with glass elements.

The first part of the report comprises two sections dealing with the behavior of glass materials under intense radiation. The first section gives data on solarization substantiating the last report showing that deterioration of laser performance under ultraviolet irradiation is not primarily due to coloration in the visible spectrum. Cerium added to a glass prevents visible solarization but causes a more rapid loss in output under use than found in non-cerium-containing glass. Fluorescence intensity shows little or no decrease in the deteriorated glass. The problem of laser deterioration under pumping is thus delineated but not yet explained. The second section reports the millisecond pulse energy that 1 μ platinum particles can endure without fracture is about 500 joules/cm^2.

The second part of the report comprises three more sections dealing with the performance of glass lasers. The third section of the report gives comprehensive threshold and output energy data for a number of Corning Code 0580 lasers. The data are compared with the behavior of the steady-state power predicted by Miles and Goldstein assuming a homogeneous line, a uniformly excited volume, and a single mode. The general features of the experimental results are consistent with this theory; the threshold varies linearly with $-\ln R_1R_2$, where R_1 and R_2 are cavity mirror reflectances, and an optimum output coupling exists for each level of excitation. Because the actual system has an inhomogeneous line and multimode oscillation in a nonuniformly excited volume, the agreement is not expected to be exact. The dynamic, or effective, internal loss coefficient of the medium calculated from threshold versus reflectance data on eight different laser samples ranges from 0.007 t 0.021 cm^{-1} for this glass. The earlier reported high internal loss value of 0.021 cm^{-1} is not typical but the result is included here as well. Curves of energy output versus input for different output reflectances exhibit a tendency to saturate at the highest energies, although the theory predicts straight lines. Approximately linear portions of these curves can be selected from which to plot curves of output energy versus R_1R_2 for fixed excitation. At low excitation these results agree with calculated curves based on the loss coefficient from the threshold measurements. At the highest excitation the

experimental points fall 33% below the calculated, reflecting the saturation effect. Regarding the cause of saturation, the experiments rule out a time degradation of efficiency but do not rule out stimulated emission losses. The fourth section describes gain measurements through a pumped rod. Previously reported gain results are fit to a simple theory using the pulse shape, with good agreement. This indicates that there is no effective delay between the pump source and the build-up of the excited state. New data illustrate that a glass amplifier probed by a glass oscillator shows more gain than when probed by a narrow band oscillator (YAG:Nd) and the ratio between the two is that calculated. The results provide an experimental aid in interpreting data from non saturated amplifier operation by either method. The last section shows preliminary data on the briefrigence generated in a glass rod which could be correlated with the previously reported interferometry on a pumped rod. These results are useful for determining pulse repetition rates.

1. SOLARIZATION

1.1 Solarization Studies (TRG)

A photofluorometer was constructed in order to measure the relative spectral pumping efficiency of the absorption bands of neodymium-doped laser glass. A mor detailed description of the experiment and apparatus is described in the report for the previous period. Results are presented for an unsolarized and a solarized specimen of Corning Code 0580 laser glass. In the current period the solarized specimen was "desolarized" by baking at 350°C for 6 hours. It was observed that the desolarization did not restore the spectral pumping efficiency.

The fluorometer is a device which measures the intensity of the fluorescence of a sample of laser material under identical optical conditions of pumping for various pumping sources. In the present experiment the pumping source is the output of a monochrometer. The input to the monochrometer is chopped light from a high pressure Xenon lamp. In this experiment the fluorescence intensity of solarized and new samples are measured as a function of wavelength of the monochrometer output. The intensity of the pumping light is measured by an Eppley thermopile and beamsplitter which samples the light between the monochromator and the fluorometer.

1.1.1 Results

The results in the previous report showed relative

spectral pumping efficiency for an unsolarized and a solarized sample of Code 0580 laser glass. In the present reporting period the samples were again run for comparison; the solarized sample was baked out at 350°C for 6 hours and both samples were run again.

Fig. 1.1 shows relative spectral pumping efficiency for solarized and unsolarized samples of Code 0580 glass before and after bakeout. An increase in efficiency is noted in the 5700Å band but no appreciable restoration is noted in the other pump bands.

1.1.2 Analysis

The results reported are in agreement with what one would expect from the results in the previous report of the effect of solarization on laser output and the restoration of output by baking out the glass. The effect of solarization and bakeout on the 5300Å pump band is beyond the resolution of the present experiment. The limitation was imposed by the spectral energy distribution of the light source and the transmission of the monochromator.

The results obtained differ somewhat from those obtained previously. It was previously reported that the reduction of spectral pumping efficiency due to solarization occurred primarily in the 5300 and 5700Å pump bands. The present experiment however indicates that efficiency is reduced in the infrared pump bands as well. Based upon improved calibration procedures the later result is considered to be

more accurate.

It is also noted that the relative efficiencies of the 7400 and 8000Å pumping bands compared with the 5300Å are lower in the present experiment. This may be due to a systematic refractive displacement of either the exciting radiation or reference beam in the beam splitter.

1.1.3 Conclusions and Recommendations

The present experiment demonstrates further that the decrease of laser output due to solarization is not by an additive absorptive loss. There is still insufficient understanding about the mechanism and properties of solarization. It is felt that the measurement of fluorescence efficiency of a severely solarized glass and the determination of the functional dependence of solarization upon pump energy and rate would be useful for a better understanding of these problems. Such understanding may present a more satisfactory means than filtering to prevent or retard solarization.

1.2 Effect of Ce_2O_3 on Solarization of 0580 laser glass (CGW)

The effect of short wavelength radiation from the pump light on the visible absorption and stimulated energy output of 0580 laser glass has been given in a previous report[6]. The nature of the ultraviolet induced visible absorption in glass has been attributed to a hole trap[18]. Stroud [18] has observed and explained the effect of the Ce^{3+} and other polyvalent ions on this visible absorption, viz, that the addition of Ce^{3+}

inhibits the formation of these defects by preferentially trapping the hole. With this in mind glasses of the 0580 composition were melted with 1, 2, 3 & 5 wt % Ce_2O_3 included, respectively. The change in the absorption at 4310Å as a function of the number of solarizing shots of 4200 joules for these compositions is shown in Fig. 1.2. For comparison, 0580 glass containing no Ce_2O_3 is included. It is seen that the induced visible absorption band is reduced with increasing Ce_2O_3 content.

A number of laser rods, ¼ in. dia. 2 3/16" long, were made from small laboratory size melts for each of the glasses listed above. The resulting rods were of reasonable good optical quality insuring some basis for comparison. Energy output measurements were made before and after exposure to unfiltered pump light. A typical result is shown in Fig. 1.3 along with a cerium-free 0580 rod for comparison. Typically the output after exposure to 10 unfiltered pump flashes at 4200 joules for the Ce_2O_3-containing rods dropped off to practically no measurable output. Thus even though the solarization (induced visible absorption) was reduced as shown in Fig. 1.2, the energy output degradation was actually enhanced by the Ce_2O_3 addition. This shows that the induced visible absorption itself is not the cause of the energy output degradation although both effects are produced by the short wavelength portion of the pump light as indicated by

previous studies[6] of the effect of filtering the pump light. Furthermore the indication that Ce_2O_3 addition enhances the output decrease offers a clue to the actual mechanism for the degradation although exactly what this mechanism is, is not clear.

Fluorescence intensity measurements were made on the same rods used for energy output and the results showed, as before, no significient drop in the steady-state fluorescent intensity except for a slight decrease caused by the removal of the UV pump bands.

2. Glass Damage Under Intense Optical Radiation

Work previously reported has shown that, while Code 0580 laser glass is relatively free of platinum inclusions for a glass melted in a platinum-lined tank, still platinum inclusions do occur in this glass. An estimate of the incidence of such inclusions was obtained by inspection of twenty-one 1/8" thick polished slices of 1½" diameter laser rod under a 60 power stereoscopic microscope. A total of 26 inclusions (all metallic) was found, ranging in size from about 1 micron to 10 microns, giving an average incidence of 5.6 such inclusions per cubic inch.

With this incidence and assuming a completely random distribution, it is seen that a rod 9/32" diameter x 2 7/8" long should contain one such inclusion. If catastrophic damage results when such an inclusion is subjected to radiation from a high power laser, the damage problem becomes serious even for a glass with the low incidence of inclusions of Code 0580.

Experiments were therefore initiated to determine the potentiality for damage of various levels of energy density and to find the threshold for damage vs. size of both platinum specks and other (crystalline) inclusions in glass.

2.1 Experimental Arrangement

A laser rod of Code 0580 glass with polished cylindrical surface and flat ends, 6.10 mm diameter and 61 mm. long, was mounted on the axis of a General Electric Xenon helical flash

tube, FT-524. The laser was mounted at one end in a pin vise which also supported a filter tube of Code 3555 glass to prevent solarization and give a somewhat reduced but constant and reproducible output. The cavity was completed by dielectric mirrors spaced 34" apart, the output mirror being 85% reflecting and the other 99% reflecting. The optical alignment was checked with an autocollimator and adjusted when necessary, prior to each shot. Input power to the flash-tube was maintained at 4.6KV, giving input electrical energy of 4200 joules.

Laser output of 2 joules in a 2 millisecond pulse was measured using a TRG 101 Thermopile, which was also used in measurement of beam divergence. The diameter of the beam at the output mirror, 0.196", was determined as the minimum diameter of a metal diaphragm which would pass the beam without reduction of output power. The thermopile was then moved to successively greater distances from the output mirror to determine the maximum distance, 156 $\pm$6 inches, at which the 0.425" diameter entrance window of the thermopile would receive the beam without reduction of output power. The whole angle of beam divergence was thus determined as 1.47 milliradians.

For the glass damage studies, the laser beam was focused on the glass sample by a simple double-convex lens mounted near the output mirror. The area of the sample to be tested was located by a microscope of 50 to 100 power mounted beyond the sample. In operation, the position of the

focus was approximately located by determining the best visual focus of the light from the autocollimator passing through the system. Thin strips of metal or glass-ceramic were then positioned at and adjacent to this point and the focus of the laser beam determined by locating the position at which the minimum hole size was formed with successive shots of the laser. The microscope was then aligned on the axis of the system and positioned with this hole in sharp focus when illuminated by the autocollimator. Since it was found that the output end face of the laser rod was also in sharp focus at this time, subsequent adjustment of glass samples was simplified. The sample was adjusted horizontally and vertically to bring an inclusion to the center of the microscope field, the microscope was focused sharply on the inclusion and the double-convex lens was adjusted axially until the end face of the laser rod was also in sharp focus. It was then only necessary to move the double-convex lens 1 mm. toward the laser rod to compensate for the index difference between the autocollimator visual focus and the laser focus at 1.06μ. Coincidence of the focus of the laser beam and the inclusion was necessary, since Code 0580 glass could not be damaged in the absence of inclusions, as explained below.

2.2 Results of Damage Tests

Lenses of four different focal lengths were used for these damage tests, 2.8 cm, 8.5 cm, 25 cm and 45 c Energy density at the focal point was computed by the equation

$$E = \frac{O_1}{\frac{\pi}{4}(D^2 f^2)}$$

where E is energy density in joules/cm^2

O_j is output energy of the laser in joules

D is beam divergence in radians

f is focal length of lens in cm.

so that these values of energy density were available:

Focal length of lens, cm.	Energy density, joules/cm^2.
2.8	150,000
8.5	15,000
25.0	1,800
45.0	540

The initial damage tests were run using the 2.8 cm. focal length lens and metallic inclusions of large size from 100 microns down to 25 microns, in Code 8312 glass samples of 3.3 mm. thickness. These large inclusions in this high-lead optical glass were readily broken out. Attention was then turned to the much smaller inclusions found in Code 0580 glass, which range down to perhaps 1 micron in size. While the majority of these inclusions were metallic, three were small stones. It was found that any of these visible inclusions caused breakage with the energy density of 150,000 joules/cm^2. However, repeated trials of shots focused in the interior of Code 0580 samples showed that no breakage resulted in the absence of visible inclusions. It should be noted that rather different results occurred when the laser beam was focused on or within 0.5 mm. of the surface of Code 0580 glass, when holes of some 50 to 80 microns diameter and perhaps three

times that depth were drilled. This surface effect would no doubt be highly dependent upon degree of polish and cleanliness of the surface.

The effect of smaller energy densities was then determined, using the successively longer focal length lenses listed above. Breakage from metallic inclusions in the interior of the Code 0580 glass samples continued to result with the 8.5 cm., the 25.0 cm. and the 45.0 cm. lenses.

Fracture size for inclusions of effectively equal initial dimension was found to be dependent upon the energy density incident thereon (Figures 2.1 and 2.2). The fracture resulting for energy density of 15,000 joules/cm^2 (8.5 cm. lens) focused on a 10 to 15 micron inclusion is shown in Figure 2.1 at 6.5X magnification. An energy density of 1,800 joules/cm^2 (25.0 cm. lens) produced the fracture shown in Figure 2.2 at 28X magnification when focused on a 10 to 12 micron inclusion. The marked reduction in fracture size associated with the reduced energy density is evident.

Fracture size at a constant energy density was found to be a function of the size of the inclusion (Figures 2.3, 2.4 and 2.5). An energy density of 540 joules/cm^2 (45.0 cm. lens) was used in this series. Figure 2.3 shows the fracture resulting for this energy density focused on a 12 x 17 micron inclusion (magnification 40X). A smaller inclusion, approximately 4 x 12 microns, caused the very much smaller fracture

characterized by only 2 fracture rings shown in Figure 2.4 at 43X magnification. Finally a very small and barely detectable inclusion, of the order of 1 micron in size, gave the almost imperceptible fracture showing only one fracture ring whose photograph at 627X magnification is reproduced in Figure 2.5. This fracture ring is not very clear in this photograph and may not be visible in reproduction. However the stress pattern seen at this inclusion in a polarizing microscope is definite proof that fracture did occur.

This single fracture ring is evidence that the very minimum energy was present which could cause any glass fracture at all. The inclusion causing this minimum fracture was so small that it was just within the limit of detection. Since energy and size of inclusion, both involved in causing fracture, were simultaneously at minimum, the threshold for damage for Code 0580 was thus fairly well defined.

Evidently inclusions of size in the range near 1 micron, detectable only under some 60 power magnification, will cause breakage with energy density of some 500 joules/cm^2. Visual inspection of glass to such limit is obviously not practical in any quantity. Complete elimination of inclusions by use of a melting process which will never produce any would be the desirable goal. Such elimination must include not only metallic inclusions but also stones as well, which seemed to be just as dangerous for the limited number we have located for testing.

3. Threshold and Energy Output as Related to Output Coupling and Internal Loss (CGW)

3.1 Introduction

Laser output calculations are straightforward if certain simplifying assumptions are made,[1,2,3] but there is in the literature little detailed verification of these calculations in actual solid systems, particularly glass systems. The purpose of this report is twofold: first, to provide comprehensive output data for future design considerations and second, to determine how well the simple theory fits output data for Corning Code 0560 neodymium glass lasers. The specific points to be checked are the determination of internal loss by means of threshold measurements and the dependence of the energy output on energy input and on output coupling.

As early as 1961 Collins and Nelson estimated the internal loss of a ruby laser from threshold measurements[4] with a result consistent with scattering measurements on the early ruby crystals. (However, later studies have pointed to secondary absorption as the dominant loss in ruby.[1]) P. A. Miles calculated the internal loss of one of our early non-optical-quality neodymium glasses from threshold measurements with a result agreeing within a factor of two with direct absorption measurement.[5] In preliminary measurements we obtained by this method a loss coefficient several times the

directly measured value for Code 0580 glass.[6] Sanford et al. used this approach with a neodymium-doped borate laser to make a very rough estimate which seemed to agree with the directly measured loss.[7] The approximate and conflicting results cited provided motivation for the more elaborate test of the method reported here.

Early measurements of ruby laser energy output versus input and mirror reflectance implied the existence of an optimum output coupling.[8] M. Hercher reported theory and experiments showing that a ruby laser should have an optimum output coupling depending on the internal loss.[9] An optimum output coupling which experimentally increased with increasing excitation was reported by R. Aagard.[10] Miles and Goldstein published a theory which predicted the detailed behavior of both three level and four level single mode systems, in particular that the optimum output coupling should increase with the excitation. This general behavior was observed in measurements on Eastman Kodak neodymium laser glasses performed by P. Mauer[11] and by A. J. Casella[12], neither of whom attempted a comparison with theory. Similar preliminary results were reported from this laboratory for Corning Code 0580 glass.[6] In the present report we wish to make a quantitative comparison of our measurements with theory, realizing that only approximate agreement can be expected since the simplifying assumptions on which the theory is based do not hold strictly for the actual system. Additional improvements on the previous work are corrections for pump lamp nonlinearity

and Fresnel reflections at glass-air interfaces.

3.2 Theory

3.2.1 Dynamic Internal Loss

In principle it is possible to calculate the internal loss of the laser medium from a knowledge of the thresholds at various values of output mirror reflectance. This can be seen as follows. For threshold considerations alone the absorption and transmission of the cavity reflectors are irrelevant; it is necessary to know only the measured reflectances R_1 and R_2. The oscillation threshold condition is then

$$R_1 R_2 \, e^{2\ell(n\sigma - \alpha_i)} = 1, \qquad (1)$$

where ℓ is the length of the laser rod, n is the excess population density, σ is the stimulated emission or absorption cross section; and α_i is the effective internal absorption coefficient. In this formulation α_i includes absorption at the laser wavelength by the medium due to impurities, diffraction loss, large angle scattering by the medium, and scattering and absorption at the rod faces. It also includes geometrical effects such as refractive index gradients in the air in the cavity and irregularities in the rod faces. Eq. (1) can be rewritten

$$2\ell n\sigma = -\ln R_1 R_2 + 2\ell\alpha_i$$

and since the threshold flashlamp input energy E_T is proportional to n for fixed pump pulse shape, it follows that

$$E_T = \frac{E_{T_o}}{2\ell\alpha_i} \left[-\ln R_1 R_2 + 2\ell\alpha_i \right] \qquad (2)$$

where E_{T_o} is the threshold for $R_1R_2 = 1$. Thus α_i can be determined from the slope and intercept of the straight line drawn through a plot of E_T versus $-\ln R_1R_2$. If this slope is K the effective loss coefficient is

$$\alpha_i = \frac{E_{T_o}}{2\ell K} . \qquad (3)$$

The result of this calculation will be called the "dynamic" or effective internal loss coefficient to distinguish it from the "static" value found by measuring the transmission of a slab of the material. However, α_i does not include any loss mechanism which is equivalent to a factor in the conversion efficiency, i.e., which rises linearly with excitation. This multiplies both K and E_{T_o} in Eq. (3) by the same factor and doesn't affect α_i. For example, consider the possibility of a fraction s of the upper state population being depleted by stimulated emission into unwanted modes. Consider also the possibility of removal of photons from the desired mode by absorption of the laser wavelength in transitions from the upper laser level upward. Eq. (1) then is modified to read

$$R_1R_2\, e^{2\ell\,[n(1-s)\sigma - n(1-s)\sigma_1 - \alpha_i]} = 1, \qquad (4)$$

where σ_1 is the absorption cross section for the transition from the upper level to a higher lying level. Eq. (4) can be written

$$2\ell\, n\sigma = \frac{-\ln R_1R_2 + 2\ell\alpha_i}{(1-s)\,(1-\frac{\sigma_1}{\sigma})},$$

and the modified threshold expression is

$$E_T = \frac{1-s_o}{1-s} \cdot \frac{E_{T_o}}{2\ell\alpha_i} [- \ln R_1R_2 + 2\ell\alpha_i] \qquad (5)$$

where s_o refers to the condition $R_1R_2 = 1$. The calculation of α_i is therefore unaffected by the upper state absorption factor $1 - \frac{\sigma_1}{\sigma}$. If the value of s is independent of excitation, hence of R_1R_2, then the stimulated emission loss term drops out also. But s may be a function of R_1R_2 and cause curvature in the E_T versus $- \ln R_1R_2$ plot.

3.2.2 Output coupling and total energy output

According to Miles and Goldstein[1] the output power for steady-state conditions is proportional to

$$[SS_o^{-1} - (1+\beta)] \beta(1+\beta)^{-1}, \qquad (6)$$

where SS_o^{-1} is the excitation power normalized to the threshold excitation power S_o for $\beta = 0$. The quantity

$$\beta = \frac{\ln(1-A_1)(1-A_2) - \ln R_1R_2}{2\ell\alpha_i - \ln (1-A_1)(1-A_2)} \qquad (7)$$

is the output coupling factor for the special case of a plane parallel Fabry-Perot cavity with mirror reflectances R_1, R_2 and absorption coefficients A_1, A_2. The length of the active material is ℓ and its internal loss coefficient is α_i. Equation (6) predicts an oscillation threshold at $SS_o^{-1} = 1 + \beta$, which is equivalent to Equation (2), and output versus input curves which are straight lines with slopes proportional to $\beta(1 + \beta)^{-1}$. This relationship is derived on the basis of a homogeneous line and a single mode in a uniformly excited volume but it is pointed out that this result is applicable to inhomogeneous lines and multimode cavities "if the oscillating mode structure and the amplified fluorescence losses from nonoscillating modes are

independent of output coupling and of excitation rate."[1] Measurements of energy output as function of input for our actual devices show a distinct departure from linearity (see, e.g., Figures 3.11 and 3.13). There are three clearly valid reasons for the upward curvature observed at lower energies. First, the theory refers to steady-state power output while the quantity measured is total energy output produced by a time varying pump pulse. If input pulse and output pulse shapes were identical, then total energies would be valid substitutes for powers. But as threshold is approached from above, the output energy becomes smaller more rapidly than the power. Experiments show that this effect is appreciable below about twice threshold. Second, near field patterns show that in the lasers used here oscillation begins in an annulus within the rod and spreads inward and outward from there as excitation is increased, filling the whole volume at about twice threshold. That is, the oscillating volume increases with excitation and causes a supralinear increase in output. Third, and similarly, the spectral width of the output increases with excitation[13] and produces further upward curvature of the output curve. This effect is strongest below twice threshold and tapers off gradually until at 6 times threshold it is negligible for present purposes. Now when the excitation is above the range of these three causes of nonlinearity the output energy curve should become linear and should have a slope proportional to

$\beta(1+\beta)^{-1}$. The constant of proportionality is a pumping efficiency averaged over the volume and over the line width and is independent of β. It is independent of excitation if there are no excitation-dependent losses (e.g., amplified fluorescence depending nonlinearly on excitation). Knowledge of R_1, R_2, A_1 and A_2 together with the value of α_i calculated by Equation (3) allows calculation of the relative output energies if SS_o^{-1} is replaced by $E_{in}\, E_{T_o}^{-1}$. In this last expression, E_{T_o} is a fictitious zero-output-coupling threshold based on an extrapolation of the linear portions of the E_{out} versus E_{in} curves.

While the existence of the above-mentioned causes of non-linearity could perhaps be removed experimentally by suitably limiting the oscillating volume and wavelength spread and by measuring output power rather than energy, it is at least instructive to compare existing data with some theoretical guideline.

If the output energy is plotted against output coupling factor β for a given input energy, the curve should go through a maximum at

$$\beta_{max} = \left(\frac{E}{E_{T_o}}\right)^{\frac{1}{2}} - 1 \qquad (8)$$

if the output versus input curves are linear. The output energy as a function of R_1R_2 is a similar curve whose theoretical maximum can be calculated from Equation (8) and the relation (7) between R_1R_2 and β.

3.2.3 Correction for Fresnel Reflection at Interfaces

One laser rod face and the adjacent mirror form a Fabry-Perot etalon in which the two reflectors have different reflectances. The reflectance of the combination is periodic as a function of wavenumber. A similar situation holds at the other end of the cavity, but the period of variation of reflectance is different if the spacing between rod face and mirror is different. If the spacing differs by a centimeter, e.g., the reflectance maxima coincide approximately every 1 cm^{-1} in wavenumber space. There are thus many of these coincidences across the laser line width. Oscillation will occur in modes restricted in wavenumber to these coincident maxima and all the energy will go into these modes. The effective R_1R_2 value for the cavity should therefore be the maximum of which the cavity is capable, both for threshold and for energy output considerations. The maximum reflectance of a single etalon with differing reflectance values for the two plates is given by

$$R' = \left[\frac{r_1 + r_2}{1 + r_1 r_2}\right]^2 \qquad (9)$$

where r_1 and r_2 are the amplitude reflection coefficients.[14] Each end of the laser cavity has an effective reflectance calculable from (9).

Compliance with Equation (9) will depend quite critically on alignment and laser end face parallelism. A rough idea of the necessary precision can be obtained by considering two wave fronts within the laser rod, one of which has undergone

reflection from the laser face and the other from the external mirror. They will be in phase within ¼ wavelength over a 1 cm aperture. If mirror and laser face are parallel to about 4 seconds of arc. A misalignment of several times this amount will destroy the enhancement of the effective reflectance.

3.2.4 Etalons as Reflectors

A plane parallel slab of optical glass forms a Fabry-Perot etalon with $r_1 = r_2 = (\eta-1)(\eta+1)^{-1}$. According to Equation (9) the effective reflectance is

$$R' = \frac{4R}{(1+R)^2}, \qquad (10)$$

where $R = (\frac{n-1}{n+1})^2$

The same arguments as used in the previous section indicate that etalons of high refractive index could be used to produce moderately high effective reflectance output mirrors. Optical quality must be good and the faces parallel to a few seconds.

3.3 Experimental Details

The experiments were performed with a TRG Model 106 Laser Power Source, Pulse Forming Network and Flash Head. This system employs two EG&G FX-47A flashtubes in a double elliptical pumping enclosure mounted between external mirrors. Four 375 μF capacitors were available and voltages up to 4 kv. The pulse length for 375 μF was about 0.5 msec and for 1500 μF about 1.5 msec. The onset of laser oscillation was detected with

photomultiplier and oscilloscope.

3.3.1 Optical alignment

The laser rods used are described in Table I. Except as noted, the ends were uncoated and side walls unpolished. If η is the refractive index, the apparent angle between the two faces as viewed with an autocollimator (Davidson, Model D275) is $\eta\theta_o$ while θ_o is the actual angle. Since this angle was small for the 1 cm x 12 cm #2 the alignment was as shown in Figure 3.1(a). In this case the dielectric coated mirrors M_1 and M_2 were first made parallel by means of the autocollimator located to the left of M_1. Then the flashhead-containing laser was inserted and the left face of the laser rod, visible through the partly transparent M_2 or M_1, was made parallel to M_1. Since the laser faces are non-parallel by 4 seconds of arc, a light beam perpendicular to M_1 would be deviated by about 2 seconds for a refractive index of about 1.5. The last three lasers listed in Table I were aligned in this way also.

The other laser samples had much larger departures from parallelism and were aligned as shown in Figure 3.1(b). Alignment was performed with all components in place. The left laser face was made parallel to M_1 while M_2 was tilted so as to return the illustrated resonant beam back on itself. Thus M_2 actually makes an angle $(\eta-1)\ \theta_o$ with the right-hand face of the laser. This alignment was accurate to a few seconds of arc in most cases.

3.3.2 Threshold Criterion

The threshold criterion was consistent (i.e., about 3 out of 4 trials) single or double spiking at a given input energy, pulsing at 0.5 - 1 minute intervals. Usually E_T could be depressed (by as much as 15%) by continued pulsing at this rate. Since temperature rise and consequent geometrical changes were surely present, this probably represents an optimum configuration for lowest threshold. That is, the temperature distribution, thus distortion, becomes such as to produce a high Q for some mode. While it is possible that the mode whose Q is maximum for one threshold determination may be different from that for another determination, it seems more probable that the systematic pulsing sequence produces approximately the same configuration and optimizes the same mode for each determination. Thresholds determined in this way were reproducible to $\pm$ 4%, which is of the order of the flashtube output reproducibility.

3.3.3 Pump Nonlinearity

In these experiments it was found necessary to surround the laser rod with a u.v.-blocking filter tubing to prevent solarization. The filter tubing used was Code 3555 having a short wavelength cutoff depending on the final warming in schedule. Typically the tubing used had a sharp cutoff near 4500Å and thus passed all the neodymium pump bands from 4750Å to 8800Å with reflection loss only. In some cases the cutoff was near 5000Å and only the 5800Å to 8800Å bands were effectively

passed. The character of the xenon flashtube spectrum changes substantially with increasing input power -- shorter wavelengths are enhanced and the sharp spectral lines in the near infrared become broadened. Also, the various Nd^{3+} pump bands have different efficiencies for a given pumping configuration. Therefore it is necessary to know the flashtube behavior for each pump band. Accordingly, the relative flashtube output energy as a function of input energy was measured for each pump band and weighted according to the pumping efficiency[6] of the band relative to the other bands. Finally the overall relative pumping efficiency as function of relative input energy was calculated and is shown in Figure 2 for the case in which all bands from 4750Å to 8800Å were utilized. Unit efficiency was assigned to an input of 400 joules from a 375 μF capacitor charged to 1460 volts. The capacitance was kept constant at 375 μF.

The above computation of overall relative pumping efficiency is based on measurements made in this laboratory except for the assumption of a flat flashtube spectrum at the reference input energy of 400 J. Good spectral data on flashtubes are not plentiful in the literature and this estimate of a flat spectrum is based on data for a smaller tube under similar conditions of loading (General Electric FT-91).[15]

An additional correction, amounting to as much as 5%, had to be made for voltage error in the monitoring voltmeter on the capacitor charging circuit. All threshold values reported

here have been corrected for voltage errors and pump nonlinearity. The largest total correction (~10%) had to be applied to the lowest measured thresholds.

3.3.4 Mirror reflectivity

The mirrors employed belonged to a Perkin-Elmer dielectric reflector set (Part Numbers 582-1060-to 582-1069) of borosilicate glass with front and back surfaces flat to 1/10 wavelength of green light, front surface multiply-coated for the desired reflectance at 1.06μ. and back surface antireflected for 1.06μ. Reflectances were measured carefully by H. L. Hoover of this laboratory using a Beckman DK-2 spectrophotometer with reflectance attachment. The transmittances were measured on a Cary Model 14 spectrophotometer. The sum of the transmittance and reflectance of any given mirror added to a value between 0.99 and 1.00, leaving the reasonable value of less than 0.01 for absorption by the coatings. Accordingly, the reflectivity was taken to be the measured value with an error of $\pm$ 0.005.

3.3.5 Output energy measurements

Output energy measurements were made by placing a one-inch diameter lens 25 cm beyond M_2 (see Figure 3.1) and positioning a TRG Model 101 Ballistic Thermopile such that the apex of the thermopile cone was separated from the lens by three fourths of the focal length. Under the best conditions (far above threshold, all optical interfaces clearly visible with the

autocollimator, no craxing of filter tubes or other obvious deterioration of the apparatus) these measurements were repeatable within about 5%. Near threshold or under poor alignment conditions, repeatability was much worse.

3.4 Results and discussion

3.4.1 Dynamic internal loss

Threshold versus the quantity $-\ln R_1 R_2$ is plotted in Figures 3.3-9. The thresholds are corrected for voltage error and pump nonlinearity. In all except Figure 3.8, each point represents a single threshold determination. A best-fit straight line is drawn through the points and values of α_i are calculated by Equation (3) and listed in Table II. The limits or error were estimated by drawing other possible straight lines through the points. Since the 1 cm x 12 cm #2 and the 1 cm x 7.3 cm #1 had sufficiently small wedge angles to make the Fresnel correction applicable, the reflectances in Figures 3.3 and 3.9 are the corrected values R_2'. The result for no Fresnel correction is shown as a dashed line.

Figure 3.8 displays the results for a set of four nominally identical laser rods with similar wedge angles, all pulsed under identical conditions. Here each point is the average of two determinations which were considerably more consistent than the previous data. Figure 3.9 is the curve for a shorter rod pulsed under these same conditions and bears out the expected relationship that E_{T_o} is independent of rod length

and the product $2\ell K$ is constant. The higher values of α_i obtained are less reliable. The 1 cm x 12 cm #2 rod had been solarized by pulsing it without a u.v. blocking filter before the threshold measurements. The antireflected rod (1 cm x 12 cm #3) had to be aligned by viewing mirror M_2 through the rod which, because of the coatings and its small ratio of diameter to length, made alignment difficult, especially for the 98.2% and 95.3% mirrors. If these questionable high values are discounted, the average result is $\alpha_i = 0.0095$ cm^{-1} with extremes of 0.007 cm^{-1} and 0.012 cm^{-1}. On the other hand the three independent determinations of α_i for the 1.5 cm x 15 cm #2 sample are quite convincing and average to 0.0073 cm^{-1} with sufficient error to overlap the statically determined value[16] $\alpha = 0.0061 \pm 0.0002$ cm^{-1}. To decide whether α_i is simply equal to the static value or is, for reasons now obscure, of the order of 50% higher, will require more precise measurements and more precise restriction of the oscillating system.

There is room for considerable variation in the interpretation of these results. We could get $\alpha_i = 0.006$ cm^{-1} by this calculation and yet have an arbitrarily large stimulated emission loss (s = constant). Or, a slowly rising $s(E_{in})$ could cause upward curvature in the E_T versus $-\ln R_1R_2$ plot, resulting in underestimation of α_i. This would obscure some other loss actually included in α_i (diffraction loss, e.g., should be significant in oscillating filaments at threshold). In this connection, it can be stated that no curvature significant in relation to the experimental error appears in the threshold plots up to the highest threshold energy of 2700 J.

The hint of curvature seen in some of the plots may well be due to difficulty in aligning the extremely high and low-reflectance mirrors.

3.4.2 Output Coupling and Total Energy

Total energy output was found to be strongly dependent on mirror alignment. Figure 3.10 is reproduced from the previous report[6] with corrected values of effective reflectance. It shows relative energy output for the 1 cm x 12 cm #2 laser versus the angular displacement of mirror M_1 from correct alignment as described above. Curve A is for conditions of low output coupling and low excitation. The effective reflectance R_1' of M_1 was 99% and the effective reflectance R_2' of M_2 was 97%. The input energy relative to input energy at threshold E_{in}/E_T in this case was 1.04. Curve B shows the behavior for the same output coupling at the higher excitation level $E_{in}/E_T = 2.9$. Curve C was obtained for high output coupling ($R_1' = 99\%$, $R_2' = 46\%$) and a moderate excitation level $E_{in}/E_T = 2.1$. Similar results were obtained with one of the non-parallel rods, showing that the sensitivity to alignment is not due mainly to the Fresnel reflections. The laser rod itself could be tilted out of alignment by 30 seconds of arc without affecting the energy output by more than 10 per cent.

The beam spread was determined by photographing the output of an image converter placed at the focus of a 100 cm focal length lens placed in the beam. The total beam spread

for even the highest energies appeared, from this uncalibrated measurement, to be about 2 milliradians.

The output energy versus input energy curves for the 1 cm x 12 cm #2 laser are reproduced from reference 6 and are displayed in Figure 3.11. The values of R_2 with which the curves are labelled are corrected for Fresnel reflection. The corrected value of R_1 is 98.7%. The capacitance was constant at 375 μF. Each point represents the average of several measurements with a mean deviation of about 5 per cent. The difference in results for the essentially equivalent reflectances of 71.1% and 70.8% typifies the reproducibility. The nonlinearity discussed in section 3.3.2 becomes more pronounced at higher output coupling. For the 97.1, 87.6, 71.1, 70.8, and 59.2% mirrors there is a fairly linear portion of the curve above approximately twice threshold, even though the spectral broadening of the output must still be occurring in this region. For the lower reflectance mirrors the linear portion of the curve should occur at energies higher than were used here. Since we see only the upward curving part of these curves they appear to have smaller slopes than the curves for higher reflectances. The nearly linear portions of the higher reflectance curves were chosen to make the most reasonable comparison with theory. The data of this figure are replotted in Figure 3.12 as energy output versus $R_1'R_2'$ with $E_{in}\ E_{T_o}^{-1}$ as parameter. Here E_{T_o} is extrapolated from the linear output

curves as explained earlier. Smooth solid curves are drawn through the experimental points. The points corresponding to nonlinear portions of the curves in Figure 3.11 are encircled to emphasize that they are not expected to fall on the theoretical curves. In computing the dashed theoretical curves, $A_1 = A_2 = 0.005$ is used, as a reasonable guess based on the discussion of Section 3.3.4. Extrapolation of input-output lines gives $E_{T_o} = 400$ J and the value $\alpha_i = 0.013$ cm^{-1} produces the best fit with the experimental points. In particular the positions of the maxima (calculated locus shown as dashed curve in the figure) are in best agreement for this choice of α_i. The heights of the maxima are in acceptable agreement for the four lower curves but the upper experimental curves fall short by about 20 per cent.

Similar results for the 1.5 cm x 15 cm #2 sample may be seen in Figures 3.13 and 3.14. In this case the capacitance was 1500 μF and the total energies correspondingly higher. Each experimental point represents a single determination and the sequence of trials was from lowest energy to highest followed by repetition in reverse order. No Fresnel correction was necessary. The general features are the same as for the 1 cm rod. Output versus input curves for reflectances of 59.1, 81.6, and 95.3% have approximately linear portions which are suitable for a comparison with theory. There appears to be some falling off of output at higher excitation for the

44.9, 59.1 and 81.6% mirrors in Figure 3.15 but not for the 95.3%. Additional measurements on other samples confirm this behavior. Even stronger saturation effects have been reported for a lithium silicate glass[11], but apparently it is not observed in ruby.[17] The calculated curves of Figure 3.14 are based on $E_{T_o} = 700$ J and $\alpha_i = 0.008$ cm^{-1}, which produces the best agreement. The progressively worse agreement of the peak heights as the excitation level rises reflects the saturation effect just mentioned. The hypothesis that this saturation might be caused by thermal distortion or by a terminal state bottleneck was tested by monitoring the pump pulse with one photomultiplier and simultaneously observing the laser output pulse with another photomultiplier, with a 10 μsec integrating time to smooth out the spikes. No degradation of output power was observed as the pulse developed even for the longest input pulses (1.5 millisec, 8000J). Apparently there is no bottleneck and the thermal distortion does not reduce the total average power but merely redistributes the power among the modes.

The apparent absence of energy-dependent stimulated emission losses in the threshold experiments does not preclude their presence under the high inversion condition in which saturation is observed. Beyond this we have no clue to the mechanism of saturation.

3.4.3 Fresnel reflectance at laser faces

The values of α_i in Table II corrected for the

Fresnel reflection at the laser faces are in much better agreement with the remaining data than are the non-corrected values. Another check on the validity of the Fresnel correction was made. Figure 3.15 shows the alignment as was previously described in Figure 1 (b) for nonparallel samples. Consider point a in Figure 3.15. In this instance the 33.7% mirror was not parallel to the laser face and the effective reflectance was 33.7%. The E_T value falls nearly on the appropriate E_T versus $- \ln R_1R_2$ curve for the 1.5 x 15 cm #1 laser. On the other hand point b represents an interchange of the mirrors such that the 33.7% mirror is now parallel to the laser face and the effective output reflectance is theoretically 49.2%. The resulting threshold is correspondingly lower, but does not quite fall on the curve. It appears plausible that with an angle $\eta\theta_o = 35$ sec in arrangement a there is a small enhancement of effective reflectance and in arrangement b the enhancement does not attain the theoretical maximum. Points c and d reveal a similar situation for the 44.9% mirror. This experiment was repeated for the antireflected rod 1 cm x 12 cm #3 with no significant change in threshold.

Further confirmation of the Fresnel reflection effect can be inferred by comparing the output versus R_1R_2 curves of Figures 3.12 and 3.14 for the two lasers at equal levels of excitation. For 1.5 cm x 15 cm #2 the peak of the E_{in} $E_{T_o}^{-1} = 5.71$ curve occurs at $R_1R_2 = 0.72$. The curve E_{in} $E_{T_o}^{-1} = 5.00$

for 1 cm x 12 cm #2 peaks at $R_1'R_2' = 0.70$. If the latter reflectances had not been corrected the peak would have fallen at $R_1R_2 = 0.58$.

3.4.4 Glass etalons as output mirrors

Plane parallel slabs of optical glass of different refractive indices were fabricated and used as output mirrors. The glasses and results are exhibited in Table III. The experimental R' was determined by comparing thresholds obtained with these flats with thresholds obtained with standard reflectors. The values thus arrived at also are consistent with energy output results using the etalons. The Code 8390 sample contained optical defects, which explains its poor performance.

3.5 Conclusions

The general features of the measured output characteristics are consistent with the uncomplicated single-mode theory; the threshold varies linearly with $-\ln R_1R_2$ and an optimum output exists for each level of excitation. The data can be used to predict optimum coupling and maximum output for actual systems.

Calculation of the dynamic internal loss from threshold measurements on eight different samples suggests that the value to use for practical purposes is $\alpha_i = 0.010 \pm 0.002$ cm^{-1} but that under favorable circumstances it can be essentially equal to the static coefficient of 0.006 cm^{-1}. Output energy measurements are consistent with these conclusions. (A clear-cut demonstration of the equality of the dynamic and static losses, however, would be very desirable.

Curves of energy output versus input for different output reflectances exhibit a tendency to saturate at the highest energies. Approximately linear portions of these curves can be selected for comparison with theory. When this is done, experimental curves of output energy versus R_1R_2 agree, at low input energies, with calculated curves using α_i from threshold measurements. At the highest energy the experimental points fall 33% below the calculated, reflecting the saturation effect. Regarding the cause of saturation, the experiments rule out time variation of efficiency but do not rule out stimulated emission losses.

Correction for Fresnel reflections at the laser end faces is justified within the experimental error by both the threshold and output measurements.

TABLE I

Laser sample descriptions

Designation	Diameter cm	Length cm	$\eta\ \theta_o$ sec	Remarks
1 cm x 12 cm #2	1.0	12.5	6	solarized
1 cm x 12 cm #3	1.0	12.1	66	antireflected ends (<¼%)
1 cm x 12 cm #6	1.0	12.1	95	antireflected ends, polished side wall
1.5 cm x 15 cm #1	1.5	15.0	35	
1.5 cm x 15 cm #2	1.5	15.0	55	
1.5 cm x 15 cm #3	1.5	15.0	55	
1.5 cm x 15 cm #5	1.5	15.0	45	
1 cm x 7.3 cm #1	1.0	7.3	3	

TABLE II

The dynamic internal loss α_i computed for various samples from the figures indicated

Designation	α_i (cm^{-1})	α_i (cm^{-1}) (No Fresnel Correction)	Fig. No.
1 cm x 12 cm #2	$0.013 \pm .003$	0.020	1
1 cm x 12 cm #3	$0.012 \begin{smallmatrix}+.006\\-.003\end{smallmatrix}$		2
1.5 cm x 15 cm #1	$0.011 \pm .003$		3
1.5 cm x 15 cm #2	$0.007 \pm .002$		4
1.5 cm x 15 cm #2 (1500 μ⁻)	0.007		5
1.5 cm x 15 cm #1	0.011		6
1.5 cm x 15 cm #2	0.008		6
1.5 cm x 15 cm #3	0.012		6
1.5 cm x 15 cm #5	0.009		6
1 cm x 7.3 cm #1	0.009	0.014	7

TABLE III

Glass Etalons as Output Mirrors

Glass	η	R' (calc.)	R' (exp)	wedge
8349	1.541	0.167	.135	< 3 sec
8306	1.645	0.212	.212	< 3 sec
8390	1.786	0.273	.216	< 3 sec
8363	1.97	0.350	.302	15 sec

4. Gain Measurements

4.1 Analysis of previously reported gain vs. time measurements for 0580 glass (CGW)

In the last report[6] the gain of an 0580 laser rod was measured as a function of time into the pumping pulse. It was desirable to see if these results are consistent with a simple four-level picture. The differential equation governing the population conversion in the excited metastable state is given by

$$\frac{dn}{dt} = - \frac{n}{\tau} + Kg(t)$$

where K is a constant involving the strength of the pump and g(t) is the time shape of the pumping pulse. Fig. 7.3 of the previous report shows this time trace. This curve was fit with a least squares polynominal of fifth order to a few percent. The differential equation was then solved yielding the relative excited state population as a function of time. The computed equation was normalized to the experimental data point at 300 μsec of Fig. 7.4 of the previous report and the results are shown in Fig. 4.1. The agreement is good indicating that a simple approach to the inversion process is valid. There is no evidence of a delay between pumping to some level well above the excited state and the radiationless decay to the excited state.

4.2 Further gain measurements (TRG)

4.2.1 Introduction

The measurements of the gain coefficient of Code 0580 glass begun in the previous reporting period were continued. In the present period the experimental procedure was improved with respect to pumping pulse shape timing control. Gain coefficients were measured for trapezoidal pumping pulses of different durations and energies, and for relatively wide and narrow bandwidth probe signals. The distribution of gain in the cross section of the laser rods was also measured.

4.2.2 Description

Time resolved measurements of gain coefficient of laser glass were made by measuring the energy gain of a probe signal in a single pass through the sample. The energy of the probe signal, generated by a short duration neodymium laser is measured on at both input and output ends of the sample by means of beamsplitters and integrated phototubes (Fig. 4.2). A gain of unity is defined as the signal when the sample is not pumped. The gain is the increase of energy apparent when the sample is pumped. This procedure compensates for fluctuations between shots in the energy of the probe signal.

The glass samples measured in these experiments were cylindrical, nominally 2-7/8 inches in length and 1 cm in diameter. The barrels were etched to present a diffuse surface to the pumping radiation. The optical configuration of

the pumping enclosure was similar to that employed in the TRG Model 104 Lase. an EG&G FX42 xenon flashlamp is imaged on the laser rod by a circular cylinder reflector of approximately 2 inch diameter. The flash lamp was operated from a pulse-forming network yielding approximately trapezoidal pulses. Two different duration pulses were used, their durations measured at one half maximum intensities were 440 and 840 microseconds.

Tubes of Code 3555 yellow filter glass were installed over the glass samples to prevent cumulative solarization from effecting the results during the experiment.

Two systems of probe laser oscillators were used: a Q-switched glass laser for overall gain measurements; and a YAG laser to determine whether line narrowing occurs. The Q-switched glass laser is a rod of Code 0580 glass of similar dimensions in a pumping enclosure of the same type. Q-switching is accomplished by means of a spinning roof prism. As generation of the probe signal is dependent upon the angular position of the prism, this element therefore becomes the basis of timing for the experiment. A magnetic pickup is used to sense the position of the prism an arbritrary interval before alignment. The signal from the magnetic pickup is then used to trigger the flashlamps of both oscillator and amplifier after suitable delays. Figure 4.3 is a timing diagram of the experiment.

At 24000 rpm pulses occur from the magnetic pickup every 2.5 milliseconds at 355 microseconds prior to the alignment position. One such pulse is selected to trigger a variable delay pulse generator which is used to trigger the amplifier flashlamp. The same magnetic pickup pulse triggers a fixed delay pulse generator which triggers the oscillator flashlamp after a delay of 1 period (2.5 ms). Therefore, with the variable delay pulse generator delay set at zero, the Q-switched pulse is produced at a time equal to 1 period plus the prism angular delay (2.5 + 0.355 = 2.855 ms) into the pumping pulse of the amplifier rod. Longer variable delays introduce the Q-switch pulse at earlier times in the amplifier pumping pulse. As an extreme, the Q-switched pulse may be introduced before the amplifier flashlamp is triggered.

The YAG oscillator crystal is a cylinder 30 mm in length and 3 mm diameter coated on both ends with a high reflectance dielectric. The rod is supported inside of filter glass tubing in the pumping enclosure discribed above. For operation of the YAG a 25 microfarad capacitor is substituted for the typical energy storage. The waveform of the laser output pulse is of 32 microsecond duration at one half maximum intensity for a 10 joule stored electrical input (Fig. 4.4). The pulse is seen to develop beginning at approximately 30 microseconds after the lamp is triggered. Timing control with the YAG probe requires the use of one delay only between the

triggering of the amplifier and oscillator flashlamps.

Calibration of gain is accomplished by noting the relative amplitudes of the phototubes when the amplifier rod is not pumped.

An additional experiment was conducted to measure the gain distribution within the cross section of the laser glass amplifier. The experiment was similar to the measurement of gain using the Q-switched oscillator probe with the following exception. A circular aperature of 1 mm diameter was scanned across the output face in the vertical and horizontal direction. Gain coefficients were measured in successive 1 mm steps. The timing for this experiment was fixed near the time of maximum gain. Gain distribution is linked to uniformity of output of the laser, it infers uniformity of pump distribution within the rod as determined by a combination of the optics of the pumping enclosure, complex absorption of the rod, or refractive effects within the rod.

In all of the above experiments an interval between shots of 2 minutes was observed.

4.2.3 Results

Time Resolved Gain 840 Microsecond Duration Pump Pulse

Figure 4.5 is a plot of gain coefficient versus time. The stored electrical input energy was 990 joules. The solid line is drawn through the average value of three samples. The wave shape of the pumping pulse is shown in

the insert. The gain coefficient is seen to rise to a value of 0.05 cm^{-1} from which it decreases as the pump extinguishes.

Time Resolved Gain 440 Microsecond Pump Pulse

Figure 4.6 shows time resolved gain for four silicate glass rods. The pumping waveform is shown in the insert. Two curves are shown for stored electrical energies of 840 and 440 joules. The curve shapes were determined from an average of normalized averages of gain coefficient at both input energies.

Time Resolved Gain with YAG Oscillator Probe

Figure 4.7 shows time resolved gain coefficient for a typical Code 0580 laser rod. The pumping pulse used the 440 microsecond 440 joule pulse utilized previously. It is observed that the gain coefficient rises to a value approximately 50 percent higher than when the glass laser probe was used. The shape of the curve is similar to that in the previous experiment as expected.

Gain Distribution

Figure 4.8 presents the distribution of gain across the face of a pumped rod of Code 0580 laser glass. The curve is a normalized plot of gain coefficient, normalized to the value of the curve at the curve center. The curves are straight lines visually fit to the points. A sinusoidal variation of gain with maximum occurring approximately midway between the center and edges is suggested by the data. The

vertical scan increases in gain in the direction of the flash-lamp.

4.2.4 Analysis

Time Resolved Gain. Comparison of the results obtained with the 840 microsecond 990 joule, and the 440 microsecond 840 joule pumping pulses point towards the expected effect on laser performance. For a normal cavity we expect the laser output energy to follow input energy independently of pulse length providing that the gain on the laser is reasonably high above threshold. For a Q-switched laser the output in energy is determined by instantaneous gain at the time of switching, all other cavity constraints being equal. Pumping energy delivered a long time (compared to the lifetime) prior to Qswitching is of little consequence to the output. It is apparent therefore, that high-power, short-duration pump sources are required for efficient Q-switched operation. In practical lasers, however, this requirement is moderated by considerations of reasonable flashlamp life.

Time Resolved Gain with YAG Oscillator Probe

The shape of the gain coefficient vs. time is the same for the case with the YAG laser probe (Fig. 4.7) as for the case with the Q-switched laser probe (Fig. 4.6) as the time resolved gain of Code 0580 glass is measured in both cases. The peak value of the gain coefficient is considerably higher for the YAG probe (0.072 cm^{-1} for YAG 0.048 cm^{-1} for

glass at 440 joules input over 440 microseconds).

The result agrees with theory which predicts that a Lorentzian gain line shape probe with a Lorentzian source line shape should exhibit a gain $1/\sqrt{2}$ times the peak gain at the line center.

Gain Distribution

The relative uniformity of the gain over the laser rod face indicates uniformity of pump light absorption in the laser. The somewhat sinusoidal fluctuation of gain suggested could be real due to residual refraction effects at the cylindrical surface of the rod after etching.

4.2.5 Conclusions and Recommendations

Continuation of time resolved gain measurements are suggested in an experiment utilizing longer samples such as in longer cavities such as the TRG Model 106 or equivalent utilizing a 15 cm long 1.5 cm diameter laser rod and two flashlamps. This experiment will provide further substantiating data for the results reported here. Gain distribution in a different pumping configuration will also be of interest.

5. Induced Birefringence Measurements (TRG)

In the last semi-annual report on this program, the results of optical path length distortions in glass lasers as a result of flashlamp-induced thermal gradients were presented. In addition to the direct variations in optical path length, thermal gradients can also induce birefringence, since thermal gradients give rise to stresses. The resulting birefringence can be related to these stresses through a knowledge of the stress-optic coefficients. An experiment was designed to measure the development of this birefringence as a function of time. Thus measurements were made of the induced birefringence following the pumping pulse. These results are of primary interest for high repetition rate systems.

The importance of induced birefringence is two-fold. First, since the degree of birefringence is a function of position within the glass, it would be expected that the output polarization would be elliptically polarized with the ellipticity and axis orientation depending upon position with respect to the output aperture. Thus, a "clean" plane-polarized output will not result.

Second, if it is desired to make optical path length correction (through the use of a phase plate, for example) then the correction should be different for the two birefringence axes, and since the direction of these axes varies across the aperture, a simple phase plate will not suffice. Moreover,

the amount of birefringence changes with the radial position across the aperture.

5.1 Experimental Procedure

The experimental apparatus is shown in Fig. 5.1. The output from a He-Ne gas laser is passed through a beam-expanding telescope which increases the beam diameter so that it will fill the sample glass laser rod. The beam is then passed through a polarizer to insure 100% linear polarization of the beam, through the glass laser rod, through an analyzer crossed with respect to the polarizer, and then impinges on a ground-glass screen. Thus, in the absence of birefringence in the laser rod, the screen is dark. When the laser rod is pumped, it develops birefringence, and the initially linear polarized wave entering the rod leaves the rod "elliptically" polarized as described above. Thus, some light is transmitted through the analyzer and strikes the ground-glass screen. A 16 mm movie camera was used to record the pattern on the screen as a function of time. A negative-type film was used in order to simplify future densitometric analysis. The laser rod was pumped by two EG&G FX-47B flashlamps in an enclosure of double cylindrical geometry.

5.2 Discussion of Results

A selection group of frames extracted from the film strip is shown in Fig. 5.2. These frames were chosen as exhibiting significant changes in the pattern between frames.

The time of occurrence of each frame is indicated on the figure.

The behavior of the birefringence patterns can be explained in a straight-forward fashion. Since the pictures are actually negatives, dark regions correspond to transmission of light while light areas correspond to zero transmission. If the energy from the flashlamps were deposited in the laser rod with cylindrical symmetry, then one would expect the thermal gradients and hence the induced birefringence to have cylindrical symmetry. Thus, the orthogonal birefringence axes would correpond to radii and concentric circles. The linearly polarized electric field vector from the gas laser would then be parallel to one rod diameter and normal to an orthogonal diameter and therfore be parallel to an optical axis. Along these two diameters, the beam would remain polarized, and hence, an extinguished cross is expected in the birefringence pattern. This cross can be observed in all of the pictures of Fig. 5.2. The distorted nature of the second pattern (Fig. 5.2b) indicates that the heat disposition did not possess perfect cylindrical symmetry. However, as the rod thermalizes during the cooling process, the symmetry does clearly develop.

The ring structure of the figures can be used as an indication of the degree of the induced birefringence. Since each light ring corresponds to zero transmission, the light rings must correspond to the loci of points where the glass

rod behaves like a full wave plate. Thus, the number of rings in the pattern determines the magnitude of the differential phase shifts for the birefringence axes. The worst case is Fig. 5.2c where six rings indicate a differential index change of $\Delta\eta = \frac{6\lambda}{L}$

where L = rod length

λ = gas lasers wavelength = 6328Å

$\Delta\eta = N_o - N_e$ = birefringence

The divergence of the pattern due to the lense-like distortion discussed in the previous report can be easily observed. It is of interest to note that even after 18 seconds, considerable birefringence still remains in the rod. Thus in high repetition rate systems, cumulative effects are expected to be important.

REFERENCES

1. P. A. Miles and I. Goldstein, "Effects of Output Coupling on Optical Masers," IEEE Trans. on Electron Devices 10, 314-318 (1963).

2. A. Yariv, "Energy and Power Considerations in Injection and Optically Pumped Lasers," Proc. IEEE 51, 1723-31 (1963).

3. G. Birnbaum, Optical Masers (Academic Press Inc., New York, 1964).

4. R. J. Collins and D. F. Nelson, "The Pulsed Ruby Optical Maser," Proceedings of the Conference on Optical Instruments and Techniques, London, 1961 (John Wiley and Sons Inc., New York, 1963) pp. 441-54.

5. Private Communication

6. R. D. Maurer et.al., "Glass Laser Research," Semiannual report under Contract Nonr-3833(00), Project Code No. 7300, Order No. 306-62, Corning Glass Works (January 30, 1965).

7. J. R. Sanford, J. H. Wenzel and G. J. Wolga, "Giant Pulse Laser Action and Pulse Width Narrowing in Neodymium-Doped Borate Glass," J. Appl. Phys. 35, 3422-3 (1964).

8. T. Lee and S. D. Sims, "A Colorimeter for Energy Measurements of Optical Masers," Appl. Opt. 1, 325-8 (1962).

9. M. M. Hercher, "The Optical Characteristics of Ruby Laser Emission," Technical Report under Grant DA-ARO(D)-31-124-G139, Project 3309-P, University of Rochester (July 1963).

10. R. L. Aagard, "Measurements of the Output from a Ruby Laser with a Central Hole in One of the End Mirrors," J. Appl. Phys. 33, 2842-4 (1962).

11. P. Mauer, "Laser Material Study," AD-612 459, Final Report under Contract Nonr-3834(00), Project Code Number 7300, Order Number 306-62, Eastman Kodak Company (22 Feb. 1965).

12. A. J. Casella, "Experimental Study of Neodymium Doped Glass Laser," AD-612 885, Technical Research Rept. No. R-1748, Proj. 1A01 3001 A091A, Frankford Arsenal, Philadelphia (Feb. 1965).

13. R. D. Maurer, "Nd^{3+} Fluorescence and Stimulated Emission in Oxide Glasses," Proceedings of the Symposium on Optical Masers, New York, April 1963, (Polytechnic Press, Brooklyn, N. Y., 1963).

14. O. S. Heavens, Optical Properties of Thin Solid Films (Academic Press Inc., New York, 1955), Chapter 4.

15. General Electric Company Flashtube Data Manual, Photo Lamp Department, Nela Park, Cleveland, Ohio.

16. T. C. MacAvoy et al., "Glass Laser Research," Semiannual Report under Contract Nonr-3833(00), Project Code No. 7300, Order Nc. 306-62, Corning Glass Works, (January 30, 1964), p. 2.

17. D. Haig-Arbib, "Power Output Characteristics of Ruby Lasers," IRE(U.K.) Conference, London, Sept., 1964.

18. J. S. Stroud et al., VII Int. Glass Congress, Brussels, July 1965.

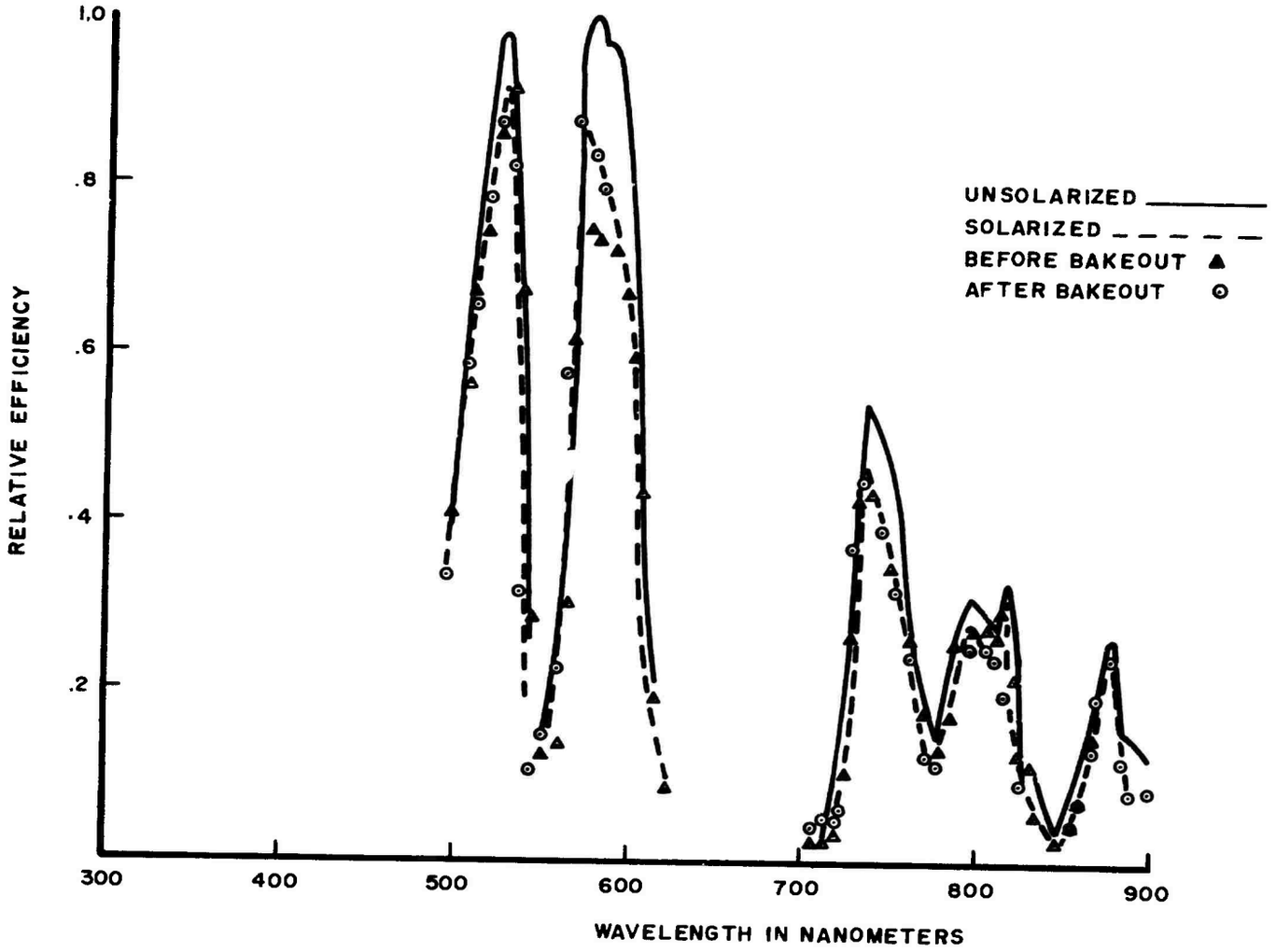

Fig. 1.1 SPECTRAL PUMPING EFFICIENCY

SOLARIZATION OF 0580 GLASS
AS A FUNCTION OF Ce_2O_3 CONTENT

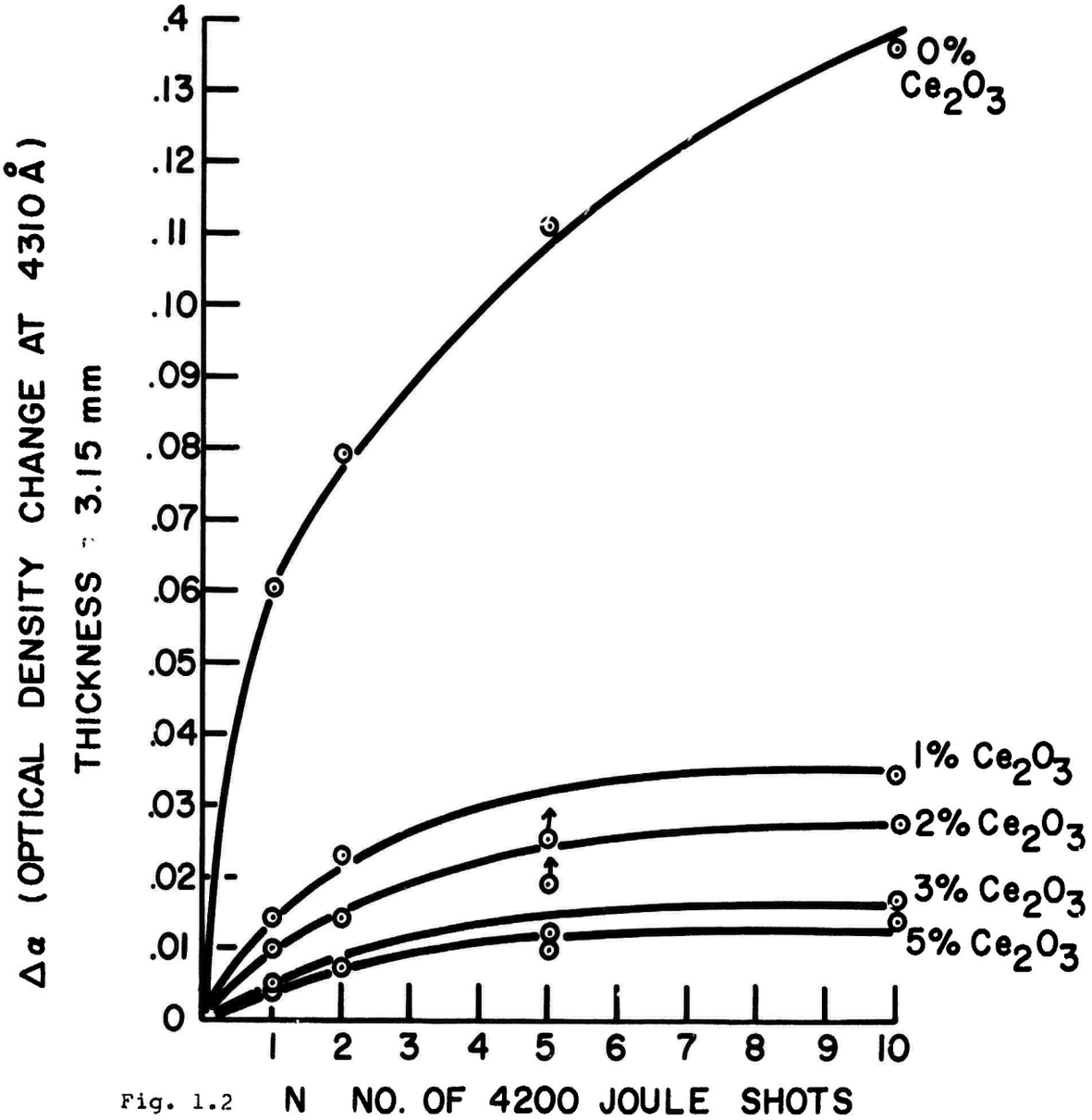

Fig. 1.2

EFFECT OF SOLARIZATION ON OUTPUT ENERGY FOR LASER CONTAINING Ce_2O_3

MIRRORS 99 – 59 %

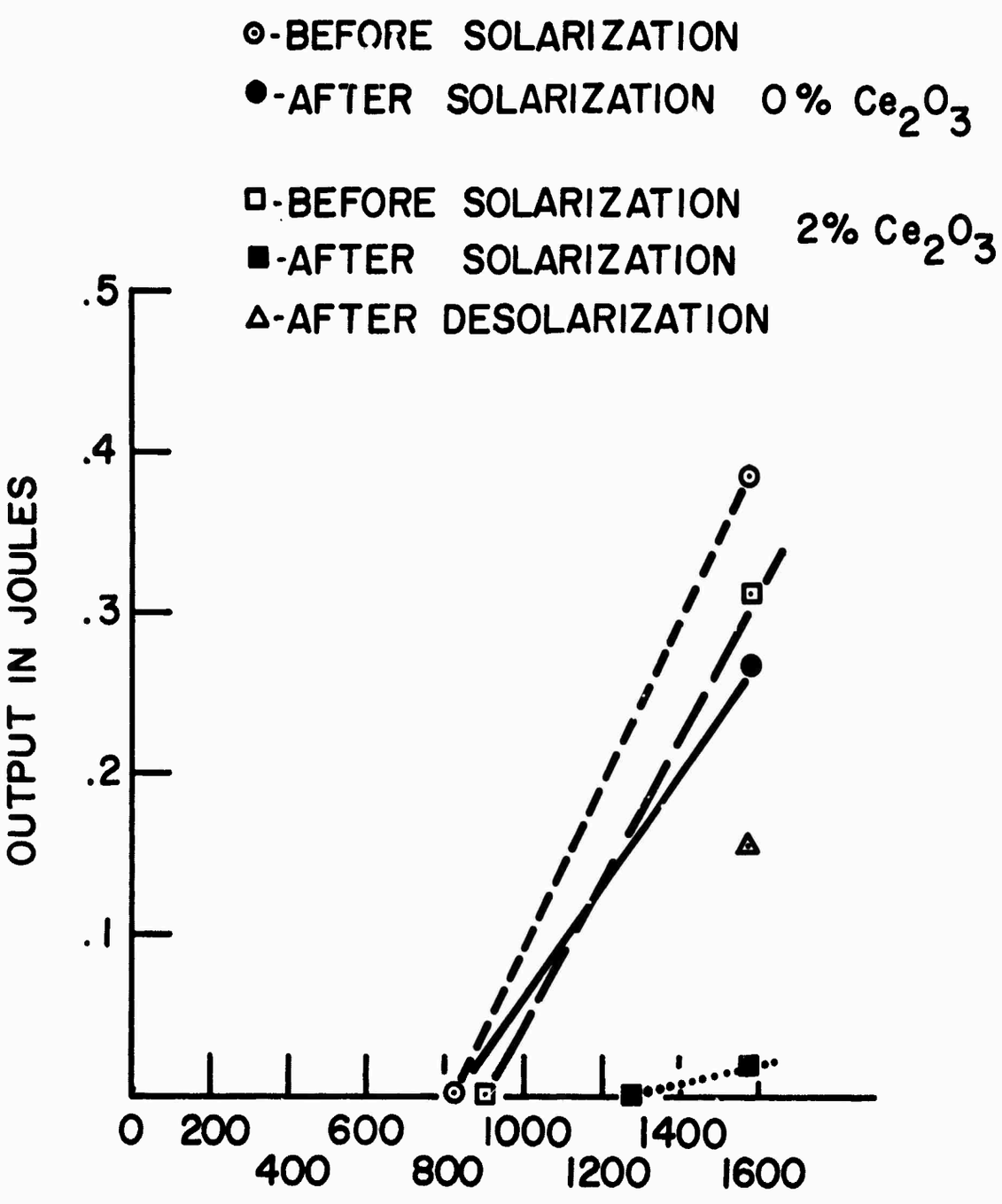

Fig. 1.3

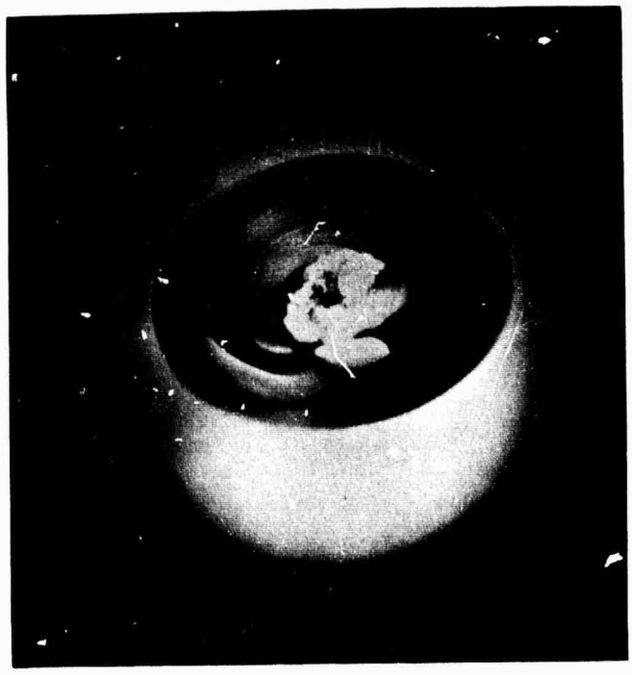

Fig. 2.1 10 to 15 micron inclusion
15,000 J/cm^2 6.5X

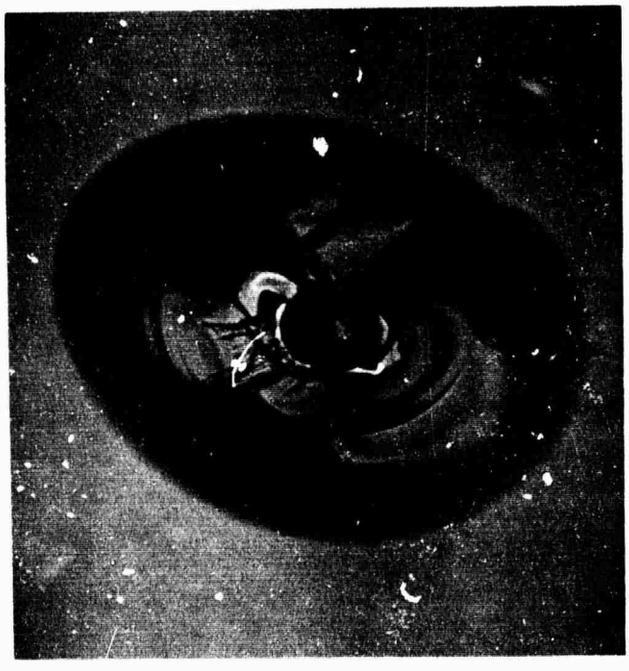

Fig. 2.2 10 to 12 micron inclusion
1,800 J/cm^2 28X

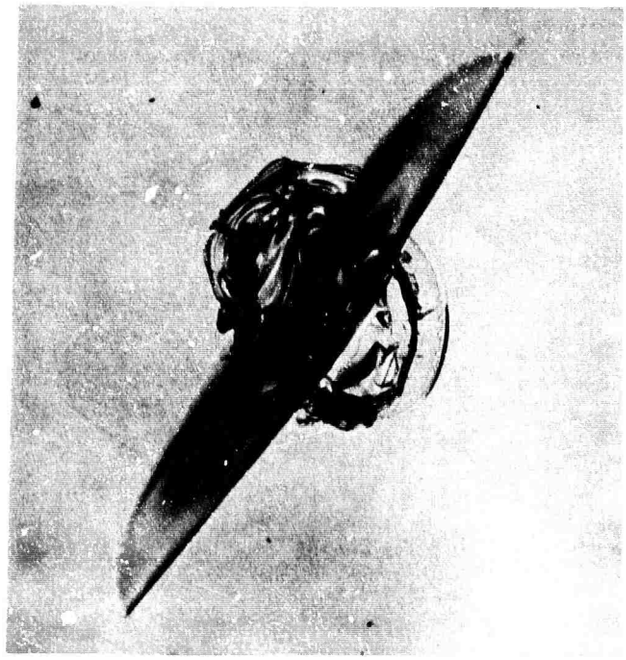

Fig. 2.3 12 x 17 micron inclusion
540 J/cm^2 40X

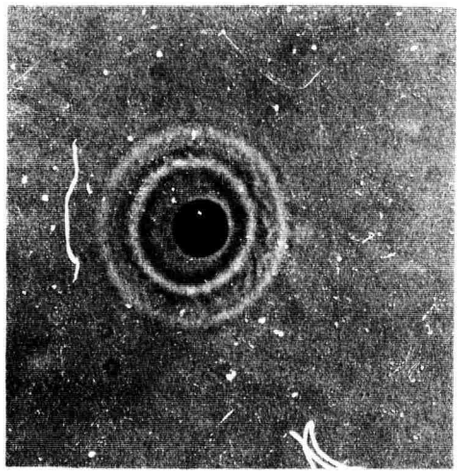

Fig. 2.4 micron inclusion
540 J/cm 434X

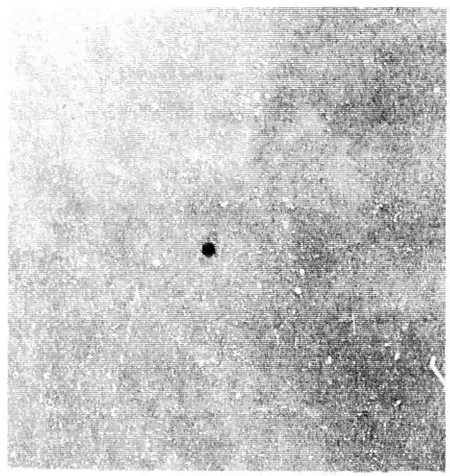

Fig. 2.5 1 micron inclusion
540 J/cm^2 627X

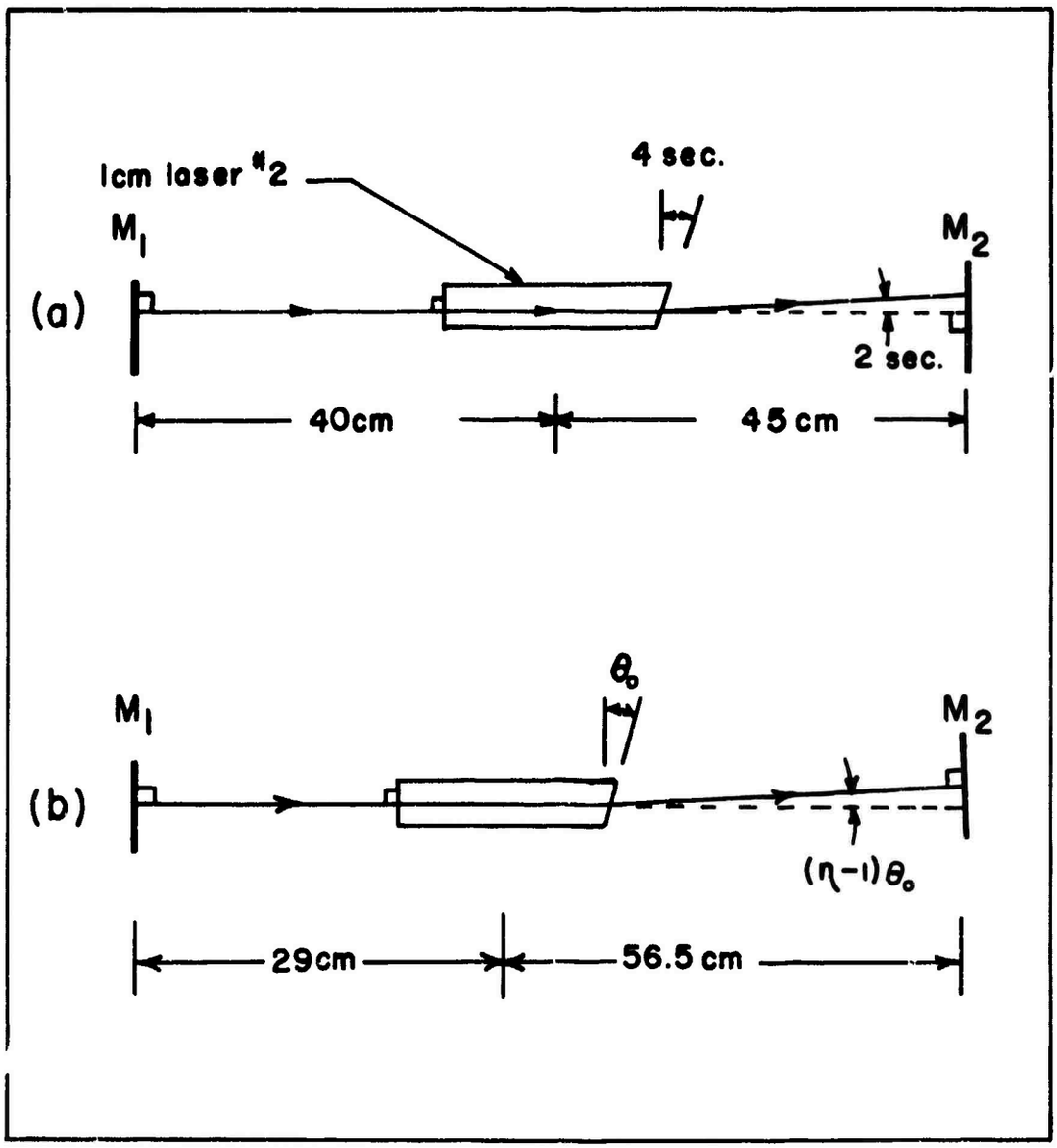

Fig.3.1 Details of optical alignment of laser cavity

(a) For laser rods with small wedge angle.

(b) For laser rods with large wedge angle.

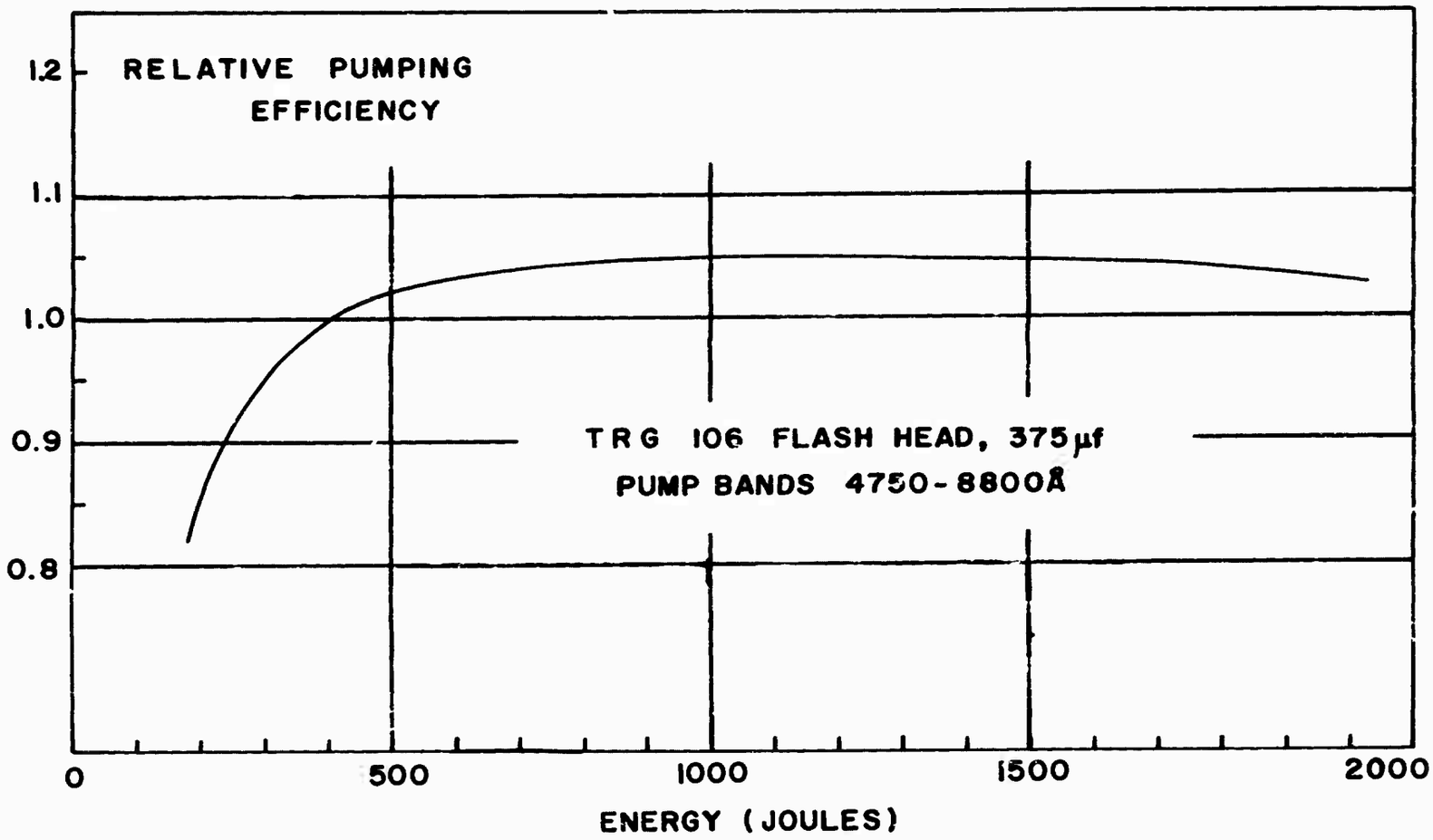

Fig. 3.2 Relative efficiency of laser pump as function of energy input.

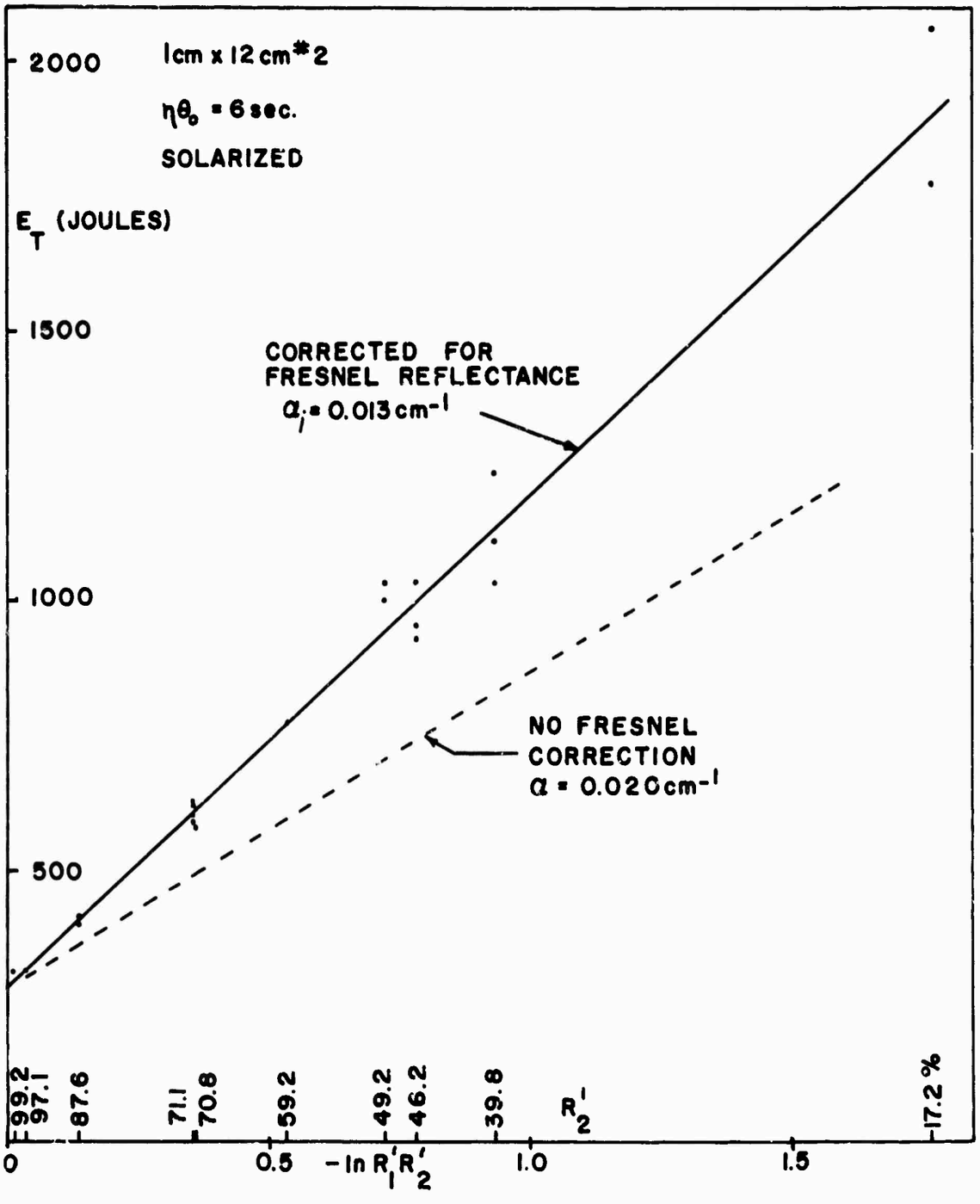

Fig. 3.3 Threshold versus $-\ln R_1' R_2'$ for 1 cm x 12 cm #2 laser rod.

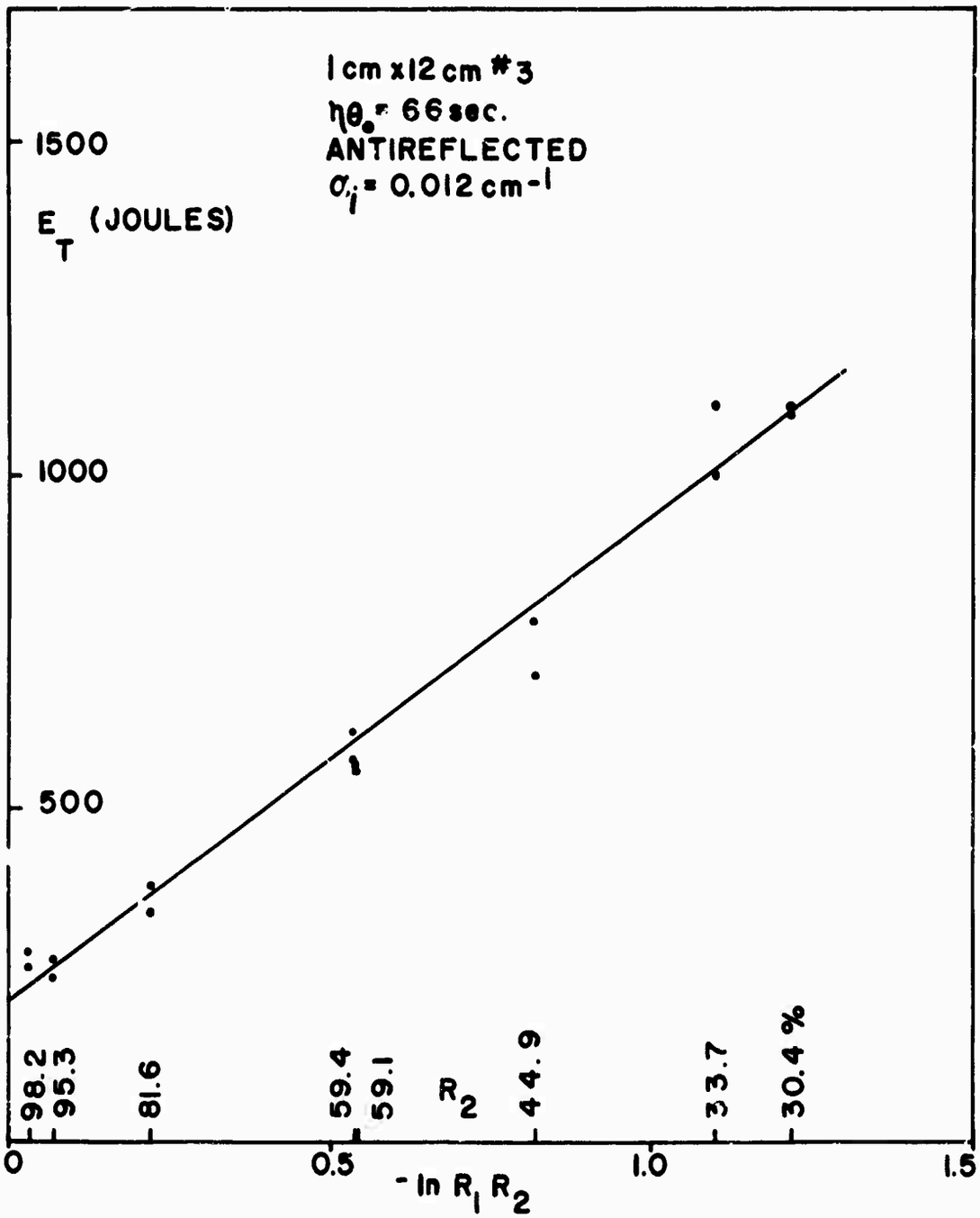

Fig. 3.4 Threshold versus -ln R_1R_2 for 1 cm x 12 cm #3 antireflected laser rod.

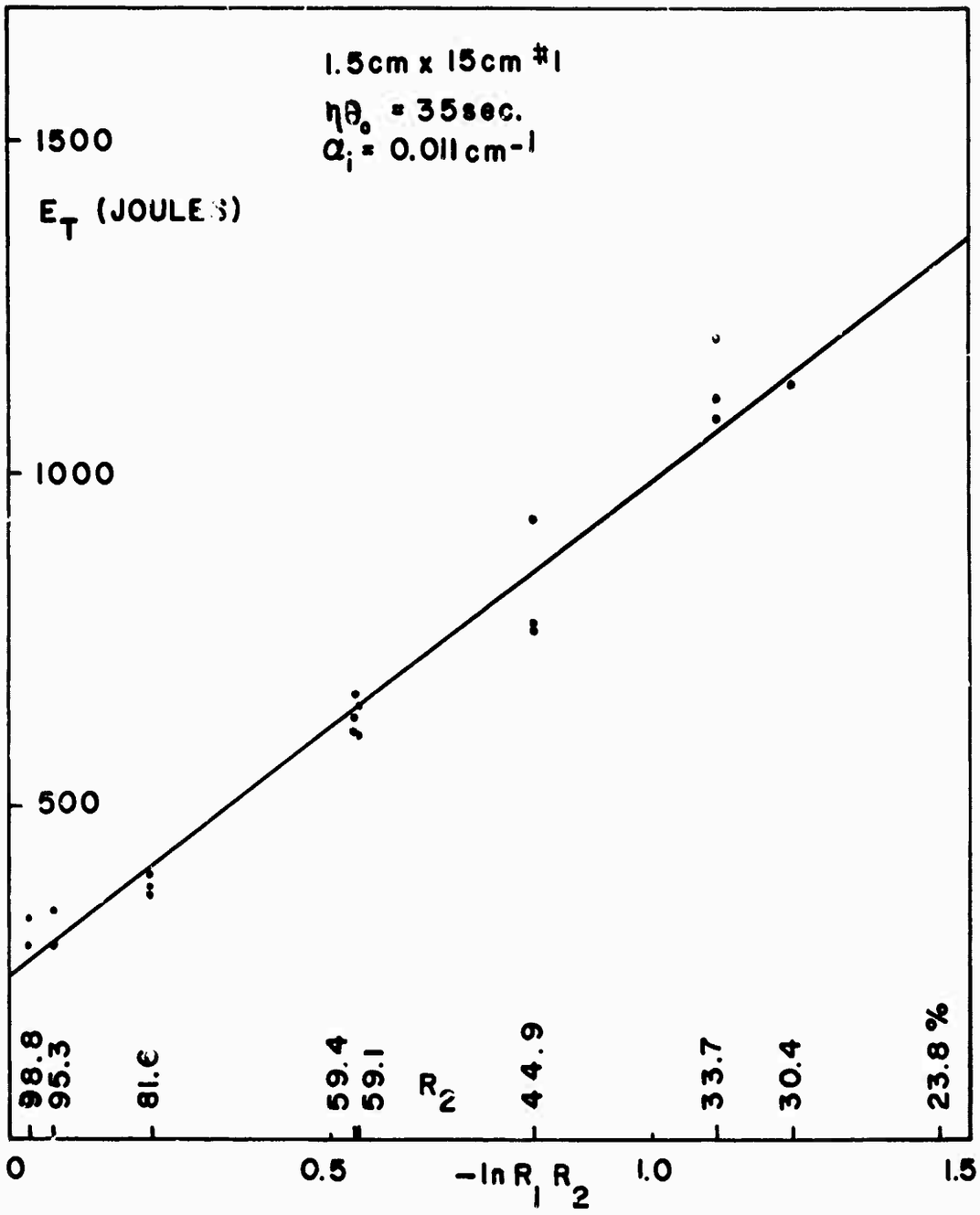

Fig.3.5 Threshold versus $-\ln R_1 R_2$ for 1.5 cm x 15 cm #1 laser rod.

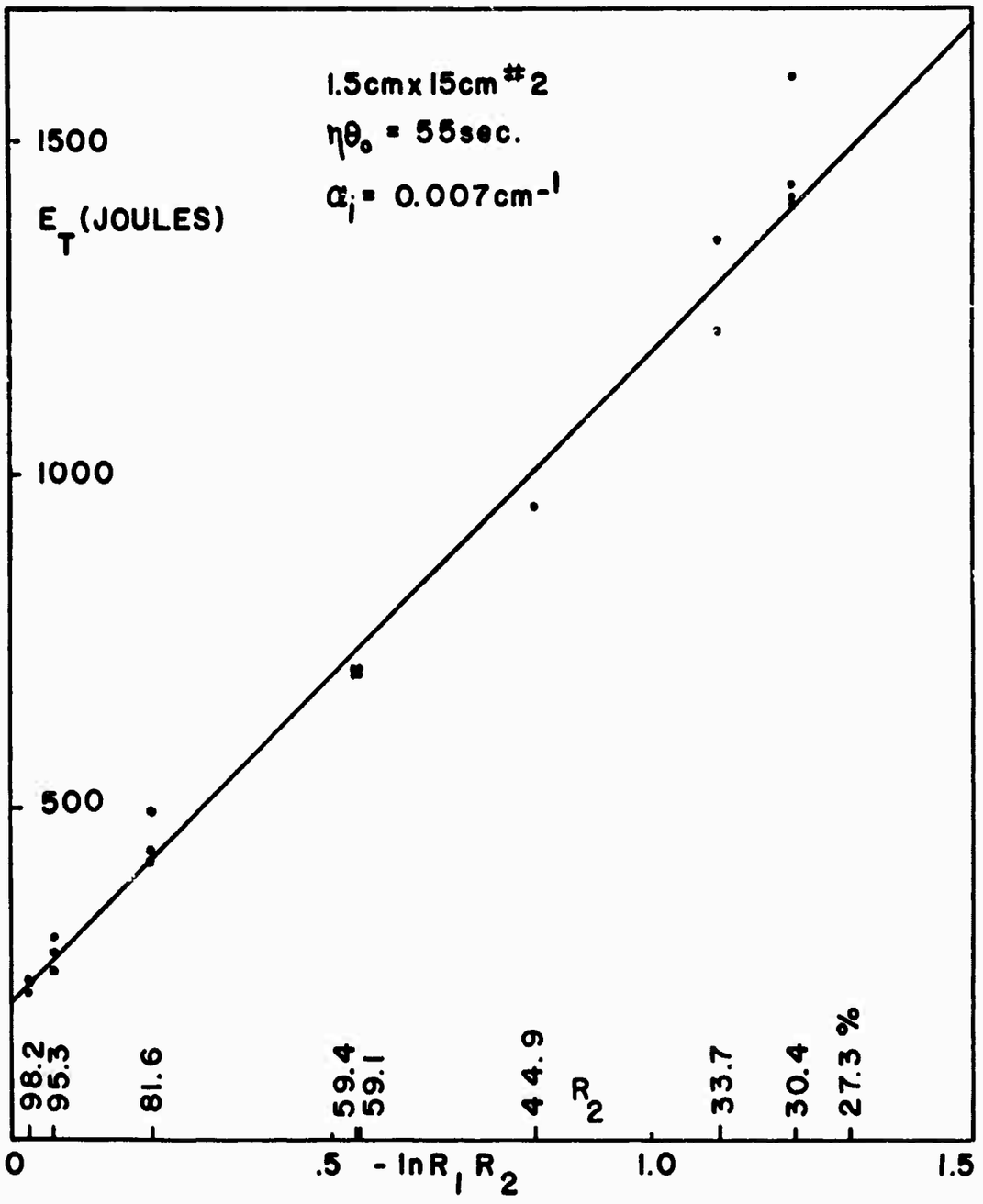

Fig. 3.6 Threshold versus $-\ln R_1 R_2$ for 1.5 cm x 15 cm #2 laser rod.

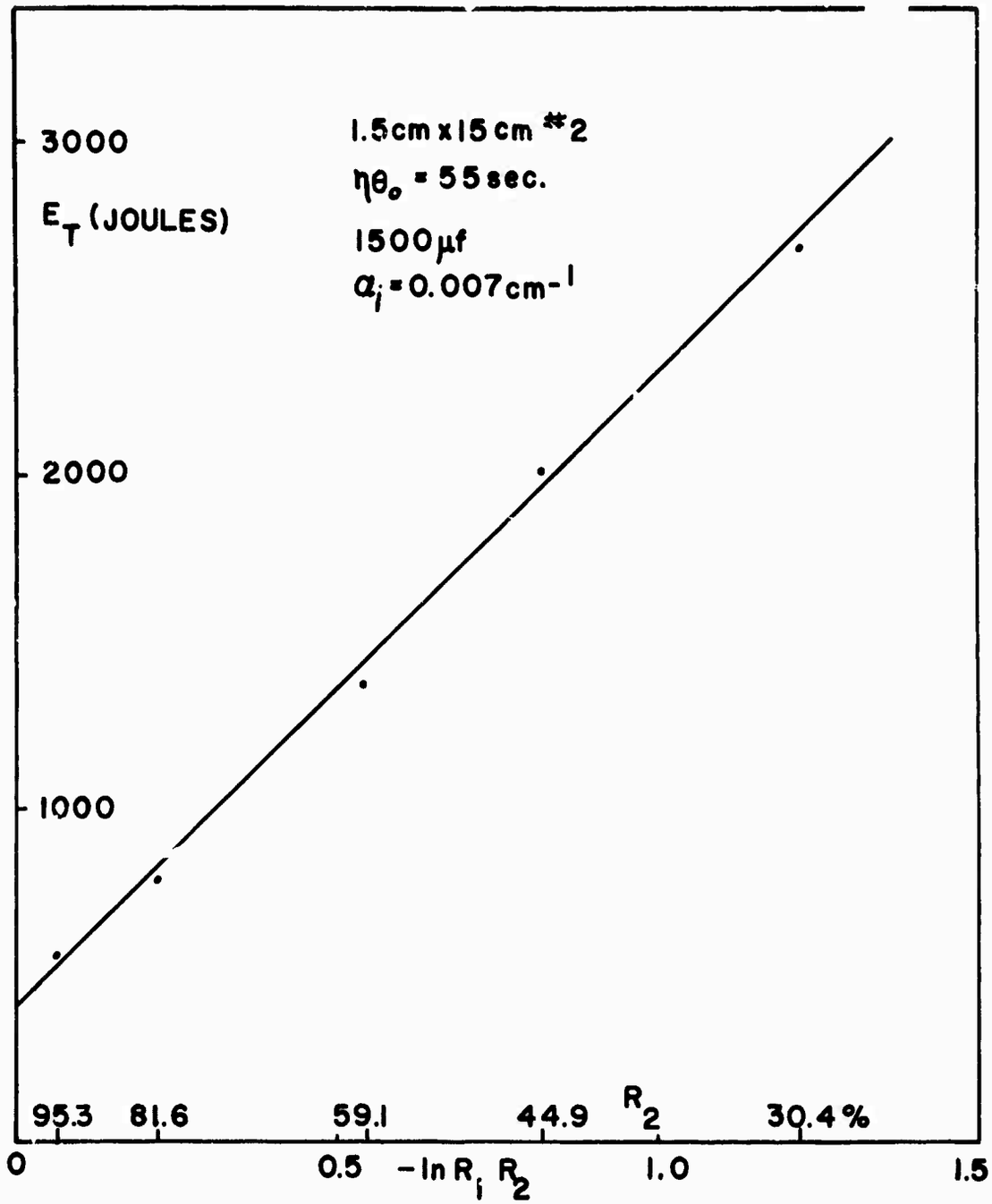

Fig. 3.7 Threshold versus $-\ln R_1R_2$ for 1.5 cm x 15 cm #2 laser rod. Capacitance 1500 μF.

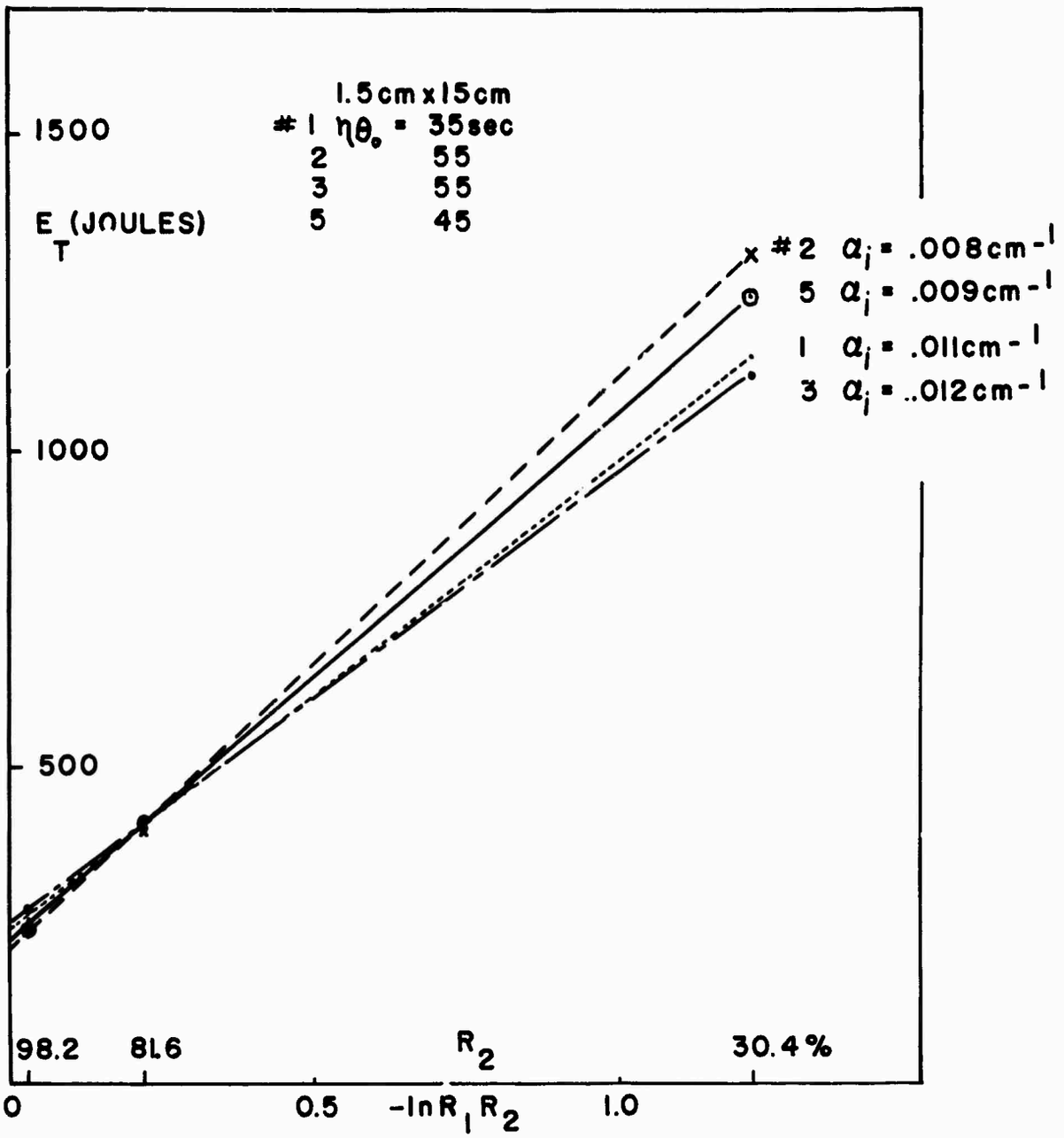

Fig. 3.8 Threshold versus $-\ln R_1 R_2$ for four nominally identical laser rods.

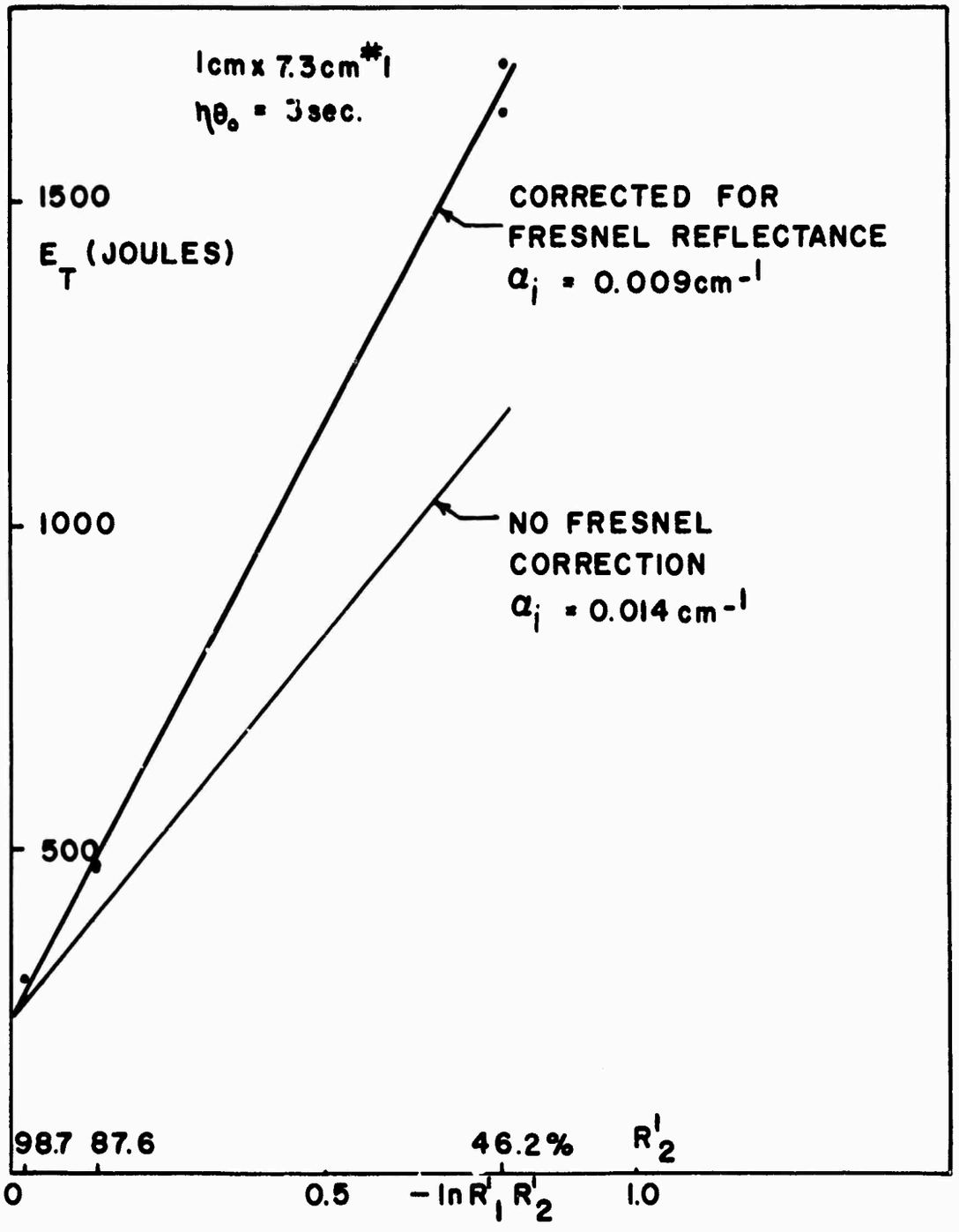

Fig. 3.9 Threshold versus $-\ln R_1' R_2'$ for 1 cm x 7.2 cm #1 Code 0580 laser rod.

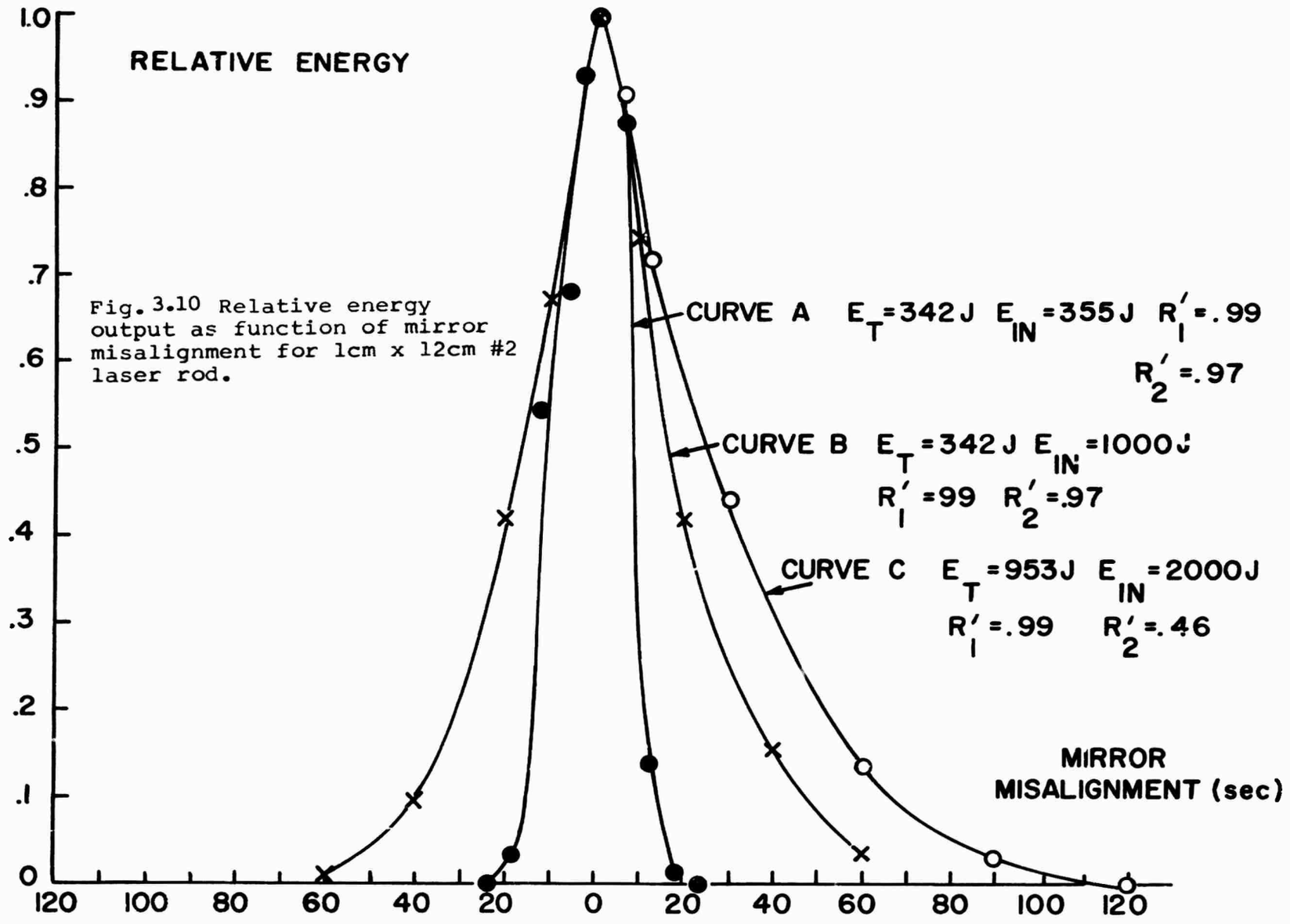

Fig. 3.10 Relative energy output as function of mirror misalignment for 1cm x 12cm #2 laser rod.

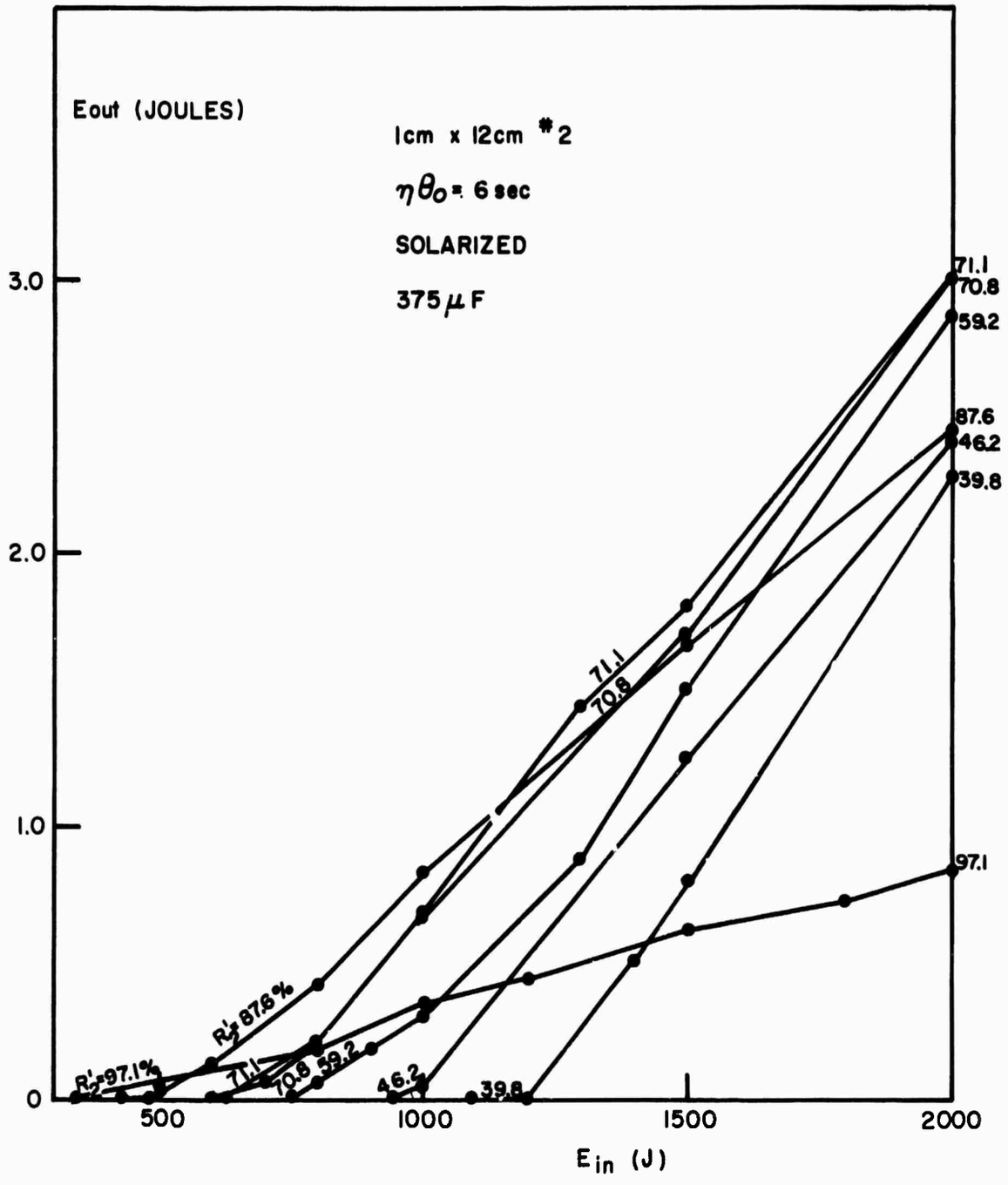

Fig.3.11 Output energy versus input electrical energy for given values of output mirror effective reflectance. Capacitance 375 μF. Laser sample 1 cm x 12 cm #2. R_1' = 98.7%.

Caption for Fig. 3.12

Output energy versus $R_1'R_2'$ for various levels of excitation for the 1 cm x 12 cm #2 laser rod. Solid lines are experimental, dashed lines calculated. The encircled experimental points come from nonlinear portions of the E_{out} versus E_{in} curves.

Fig. 3.12

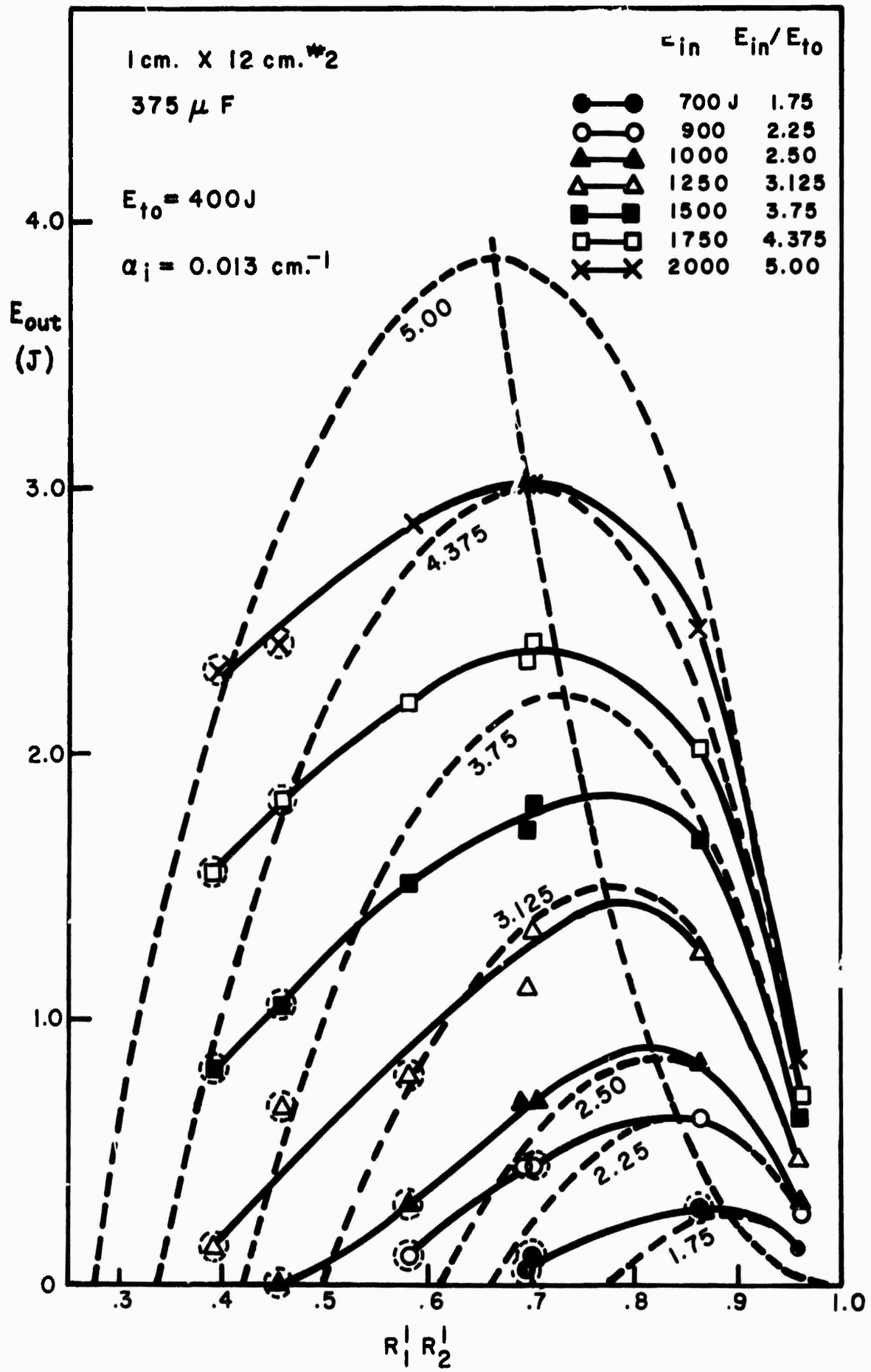
1 cm. X 12 cm.**2
375 μ F
E_{to} = 400J
α_i = 0.013 cm.$^{-1}$
E_{in} E_{in}/E_{to}
700 J 1.75
900 2.25
1000 2.50
1250 3.125
1500 3.75
1750 4.375
2000 5.00
E_{out} (J)
4.0
3.0
2.0
1.0
0
5.00
4.375
3.75
3.125
2.50
2.25
1.75
.3
.4
.5
.6
.7
.8
.9
1.0
R_1^1 R_2^1

Caption for Figure 3.13

Output energy versus input electrical energy for various output mirror reflectances for 1.5 cm x 15 cm #2 laser rod. Capacitance 1500 μF. R_1 = 98.8%.

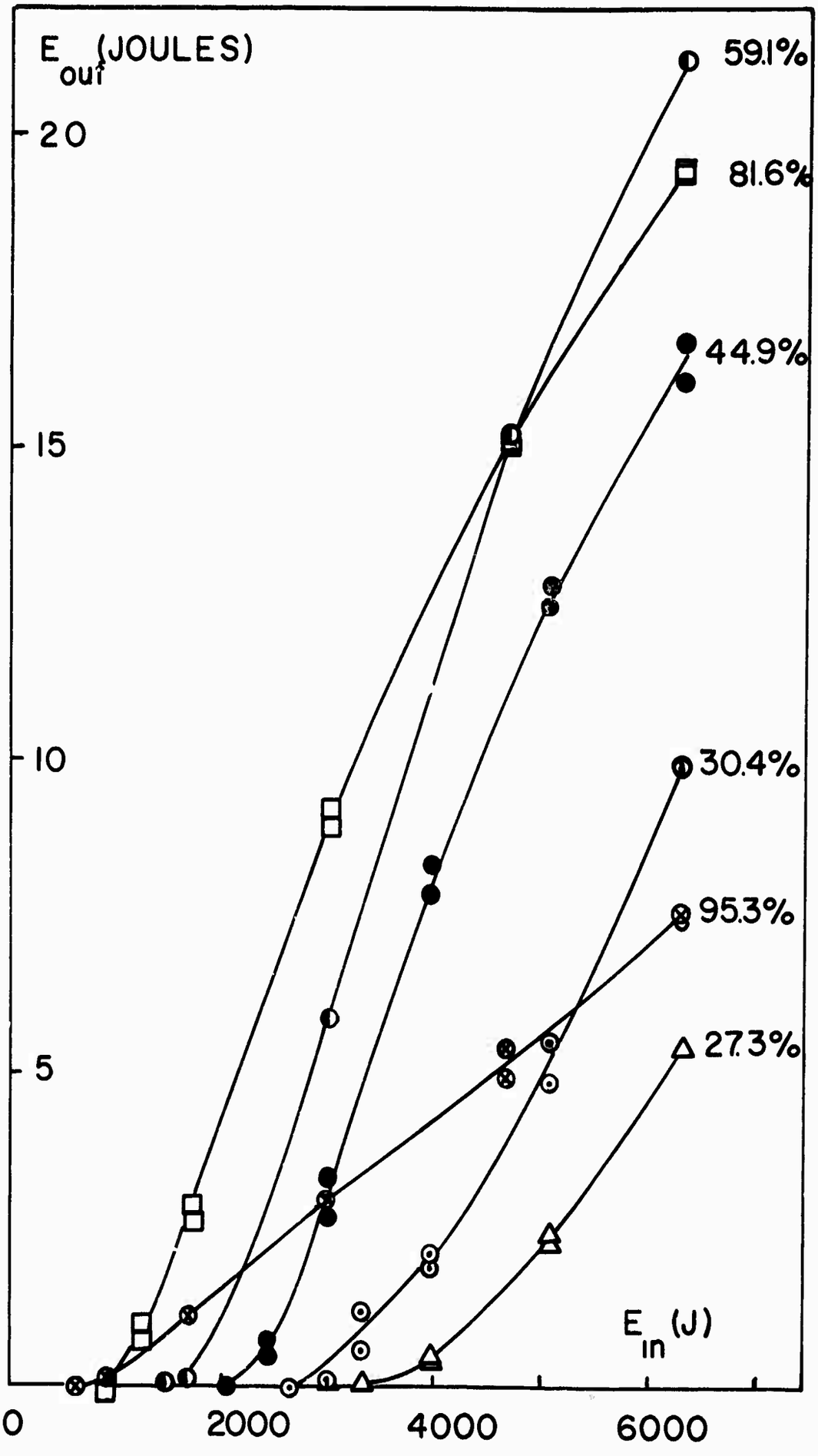
E out (JOULES)
20
15
10
5
0
2000
4000
6000
E in (J)
59.1%
81.6%
44.9%
30.4%
95.3%
27.3%

Fig. 3.13

Caption for Figure 3.14

Output energy versus R_1R_2 for various levels of excitation for the 1.5 cm x 15 cm #2 laser rod. Solid lines are experimental, dashed lines calculated. The encircled experimental points come from nonlinear portions of the E_{out} versus E_{in} curves.

Fig. 3.14

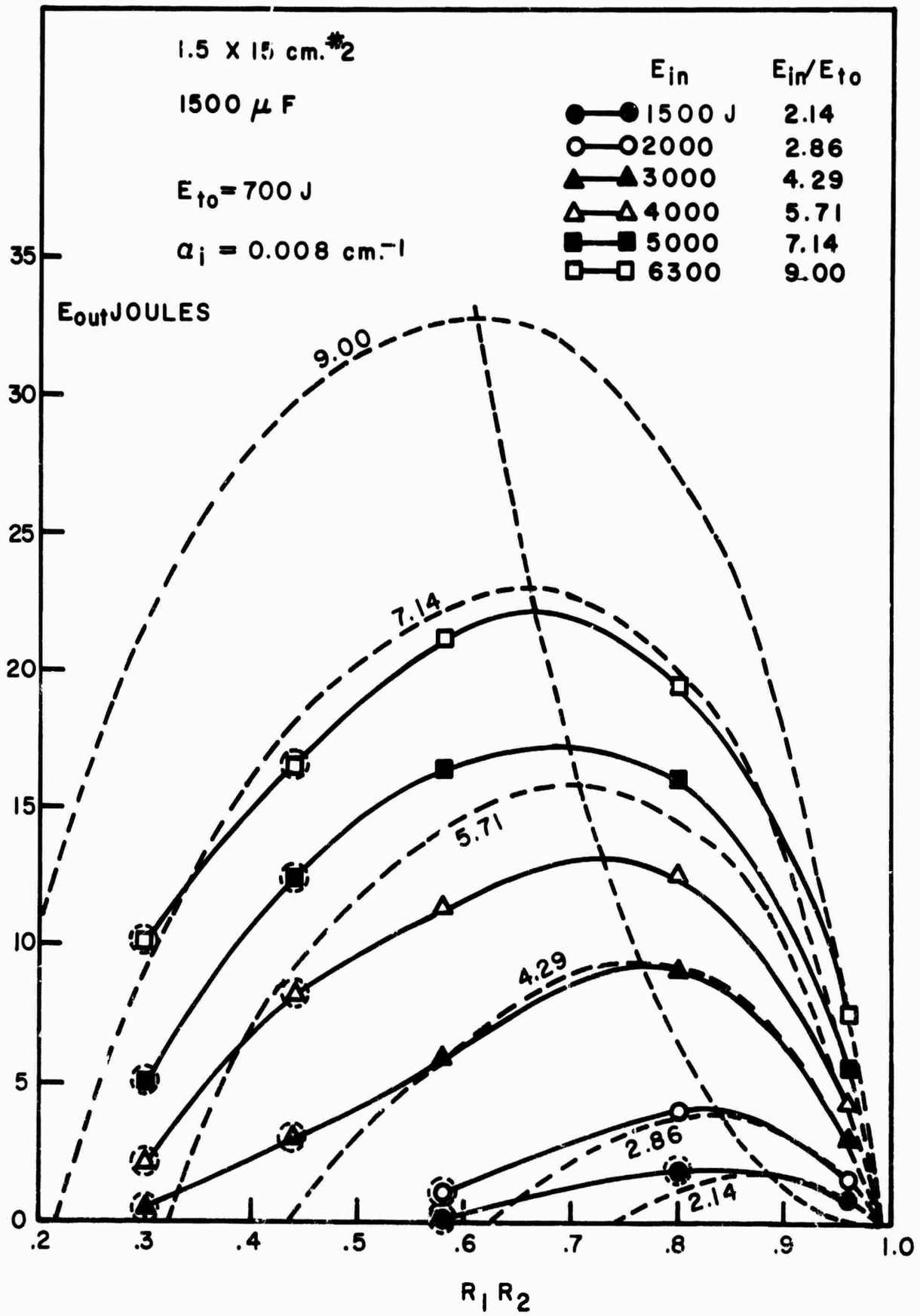
1.5 X 15 cm.*2
1500 μ F
E_{to} = 700 J
α_i = 0.008 cm.$^{-1}$
E_{in}
E_{in}/E_{to}
1500 J 2.14
2000 2.86
3000 4.29
4000 5.71
5000 7.14
6300 9.00
E_{out} JOULES
9.00
7.14
5.71
4.29
2.86
2.14
0
5
10
15
20
25
30
35
.2
.3
.4
.5
.6
.7
.8
.9
1.0
$R_1 R_2$

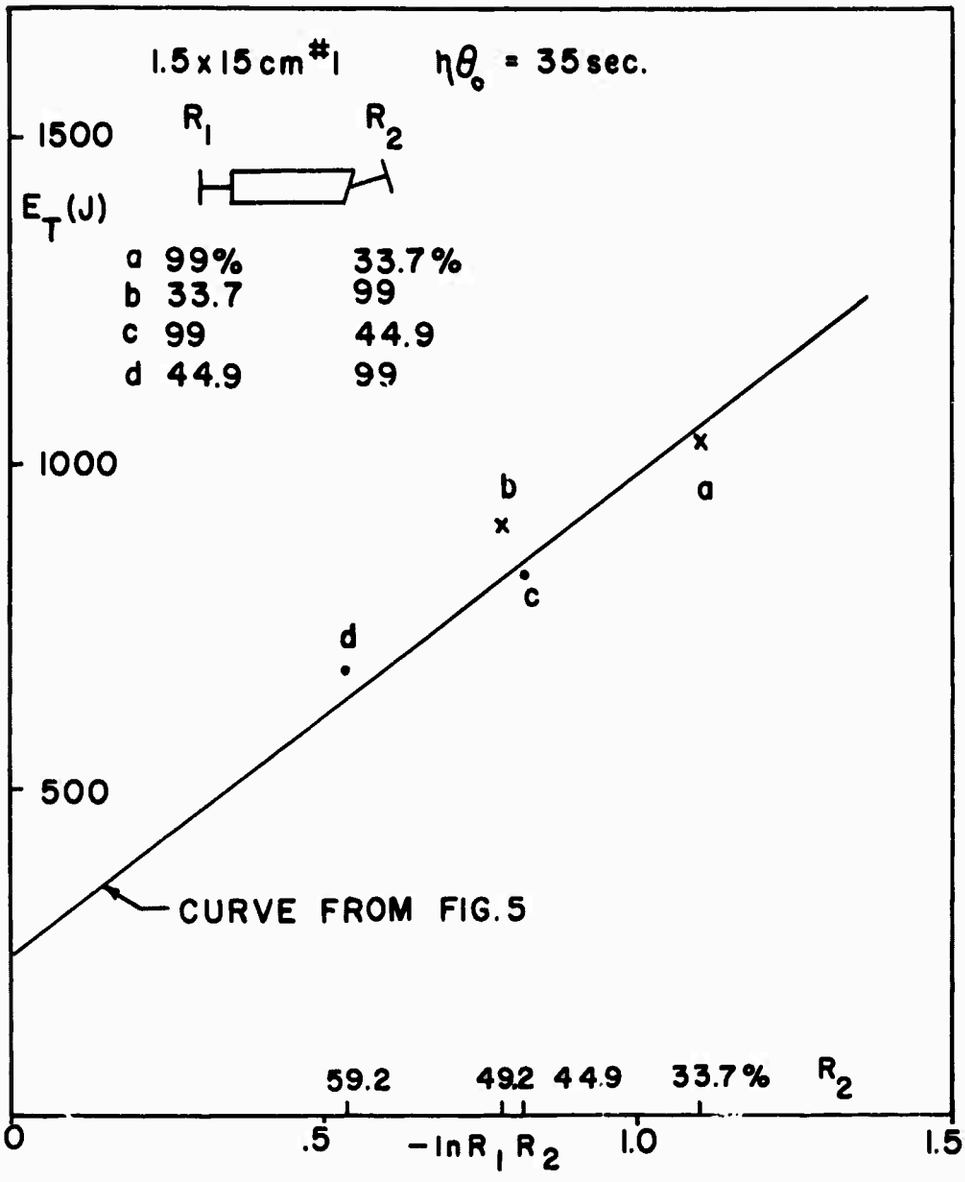

Fig. 3.15 Graph of threshold versus $-\ln R_1 R_2$ for demonstrating effect of Fresnel reflections. Laser sample 1.5 cm x 15 cm #1.

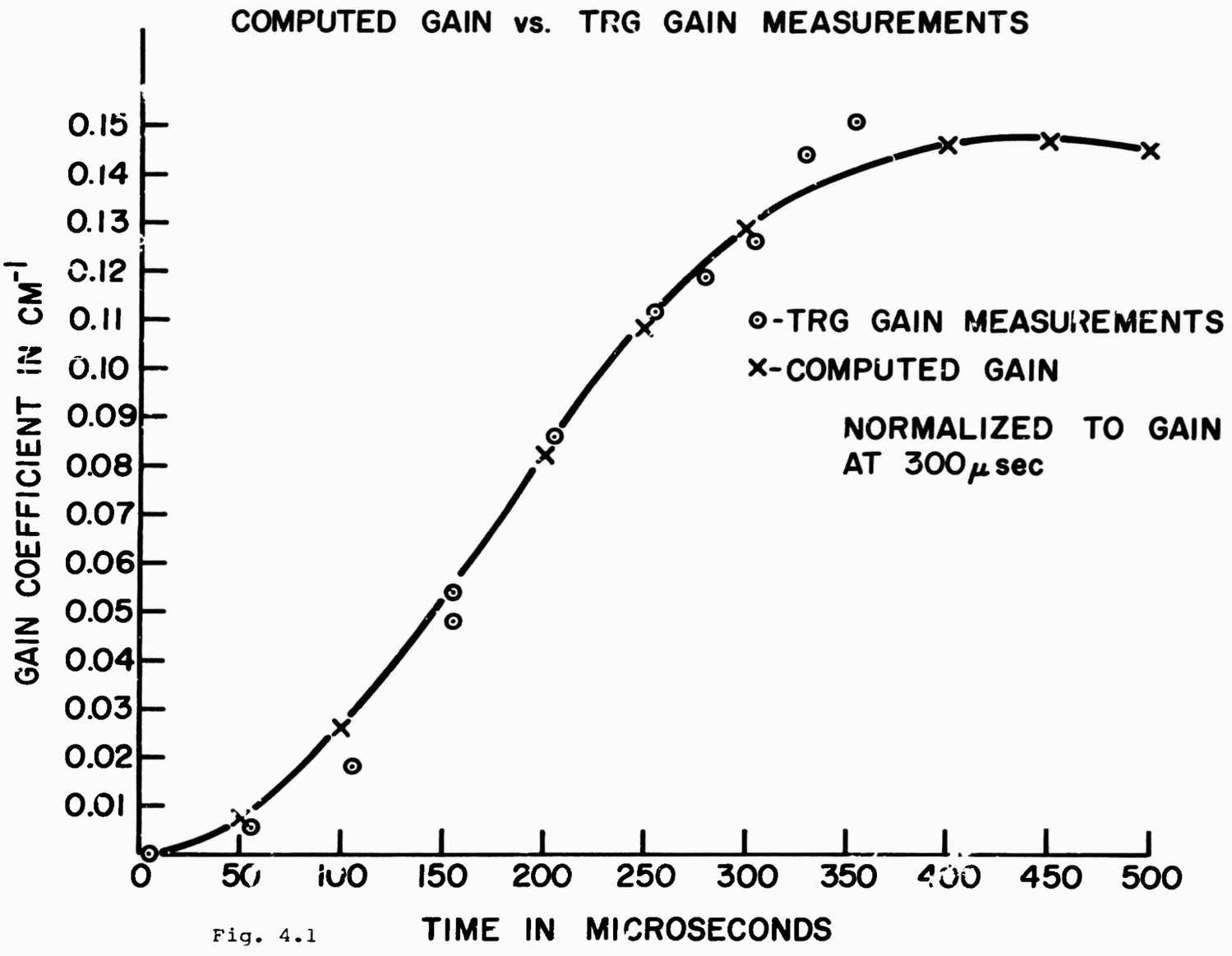
COMPUTED GAIN vs. TRG GAIN MEASUREMENTS
GAIN COEFFICIENT IN CM⁻¹
0.15
0.14
0.13
0.12
0.11
0.10
0.09
0.08
0.07
0.06
0.05
0.04
0.03
0.02
0.01
0
50
100
150
200
250
300
350
400
450
500
TIME IN MICROSECONDS
⊙-TRG GAIN MEASUREMENTS
×-COMPUTED GAIN
NORMALIZED TO GAIN
AT 300μsec

Fig. 4.1

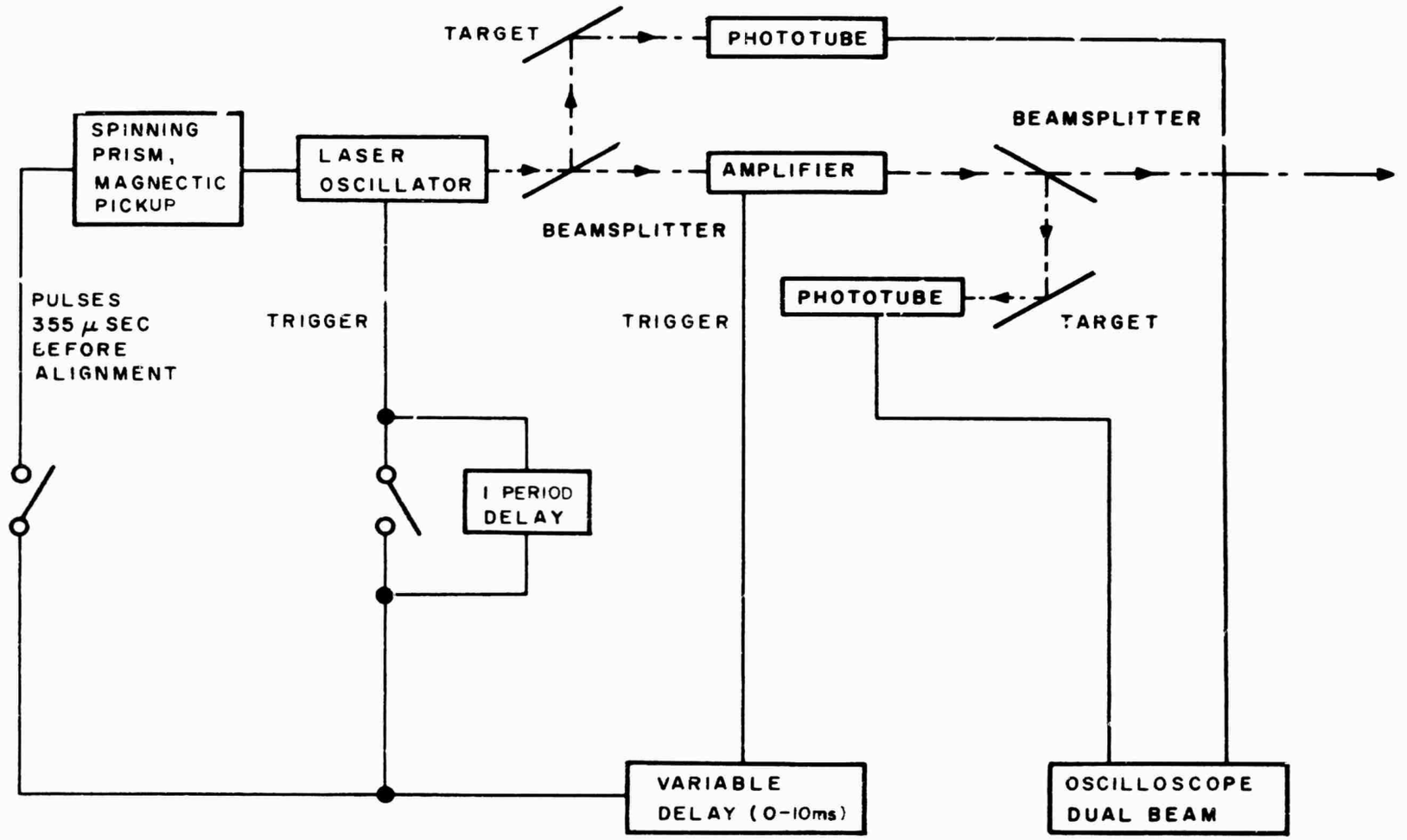

Fig. 4.2FUNCTIONAL BLOCK DIAGRAM - GAIN MEASUREMENT

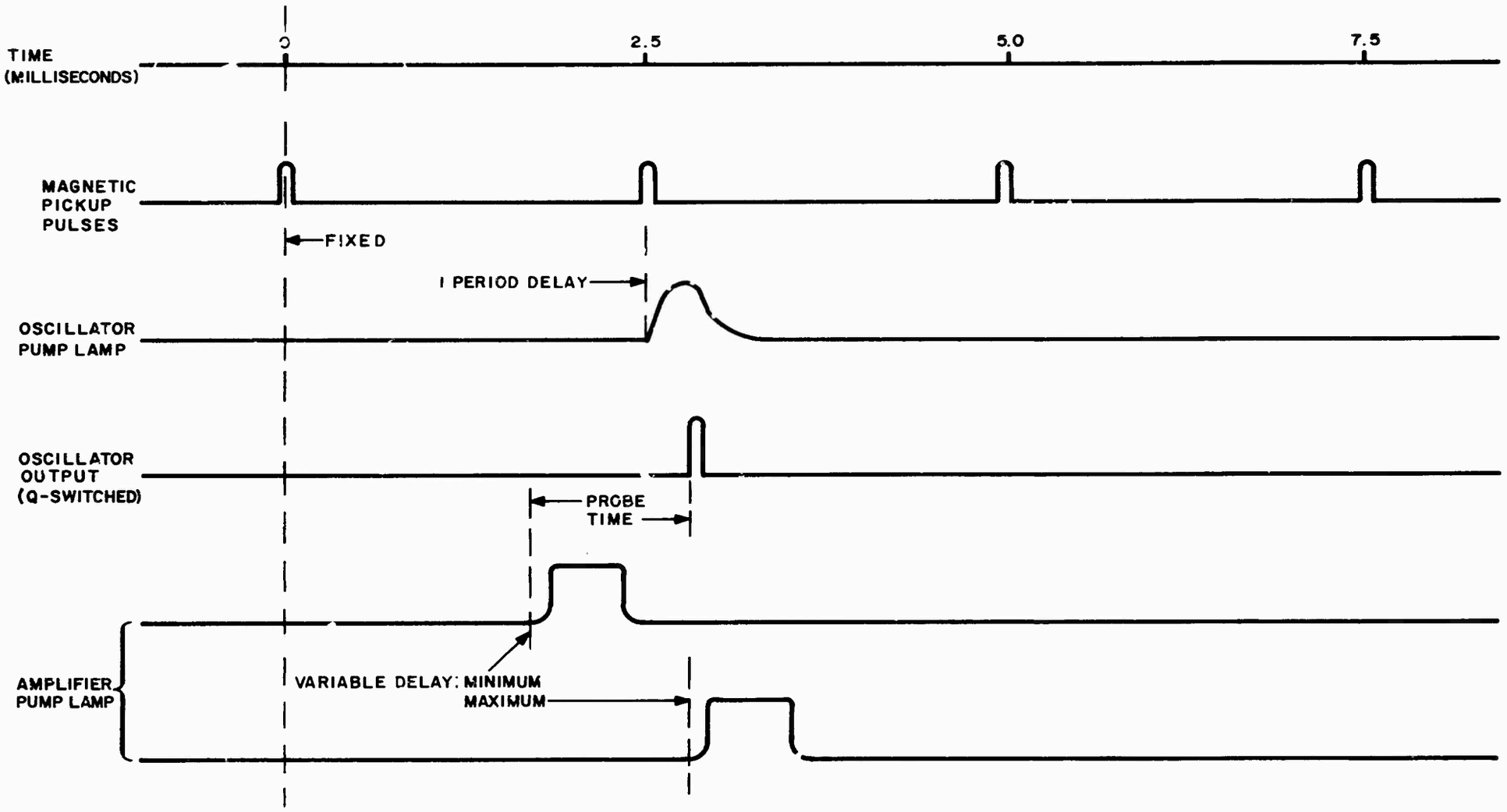

Fig. 4.3 TIMING DIAGRAM: TIME RESOLVED GAIN MEASUREMENT USING Q-SWITCHED LASER OSCILLATOR PROBE

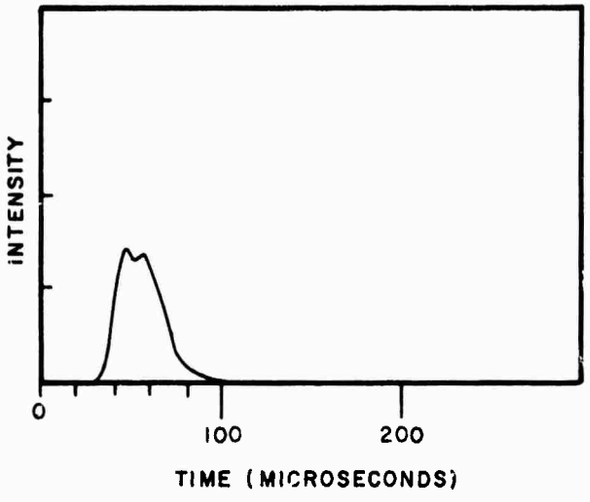

Fig. 4.4 OUTPUT PULSE SHAPE Nd YAG LASER

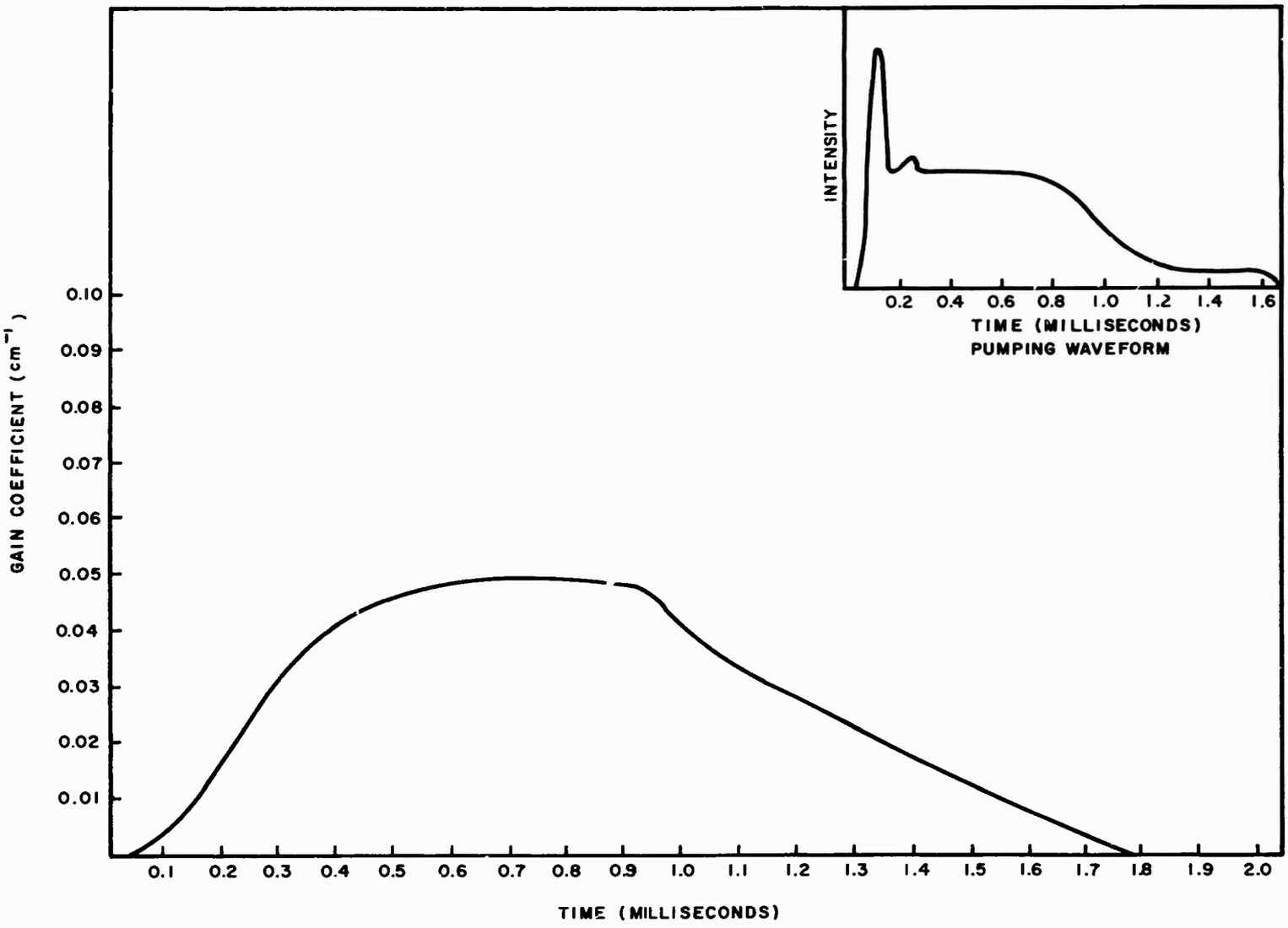

Fig. 4.5 TIME RESOLVED GAIN; 840 MICROSECOND PUMP PULSE

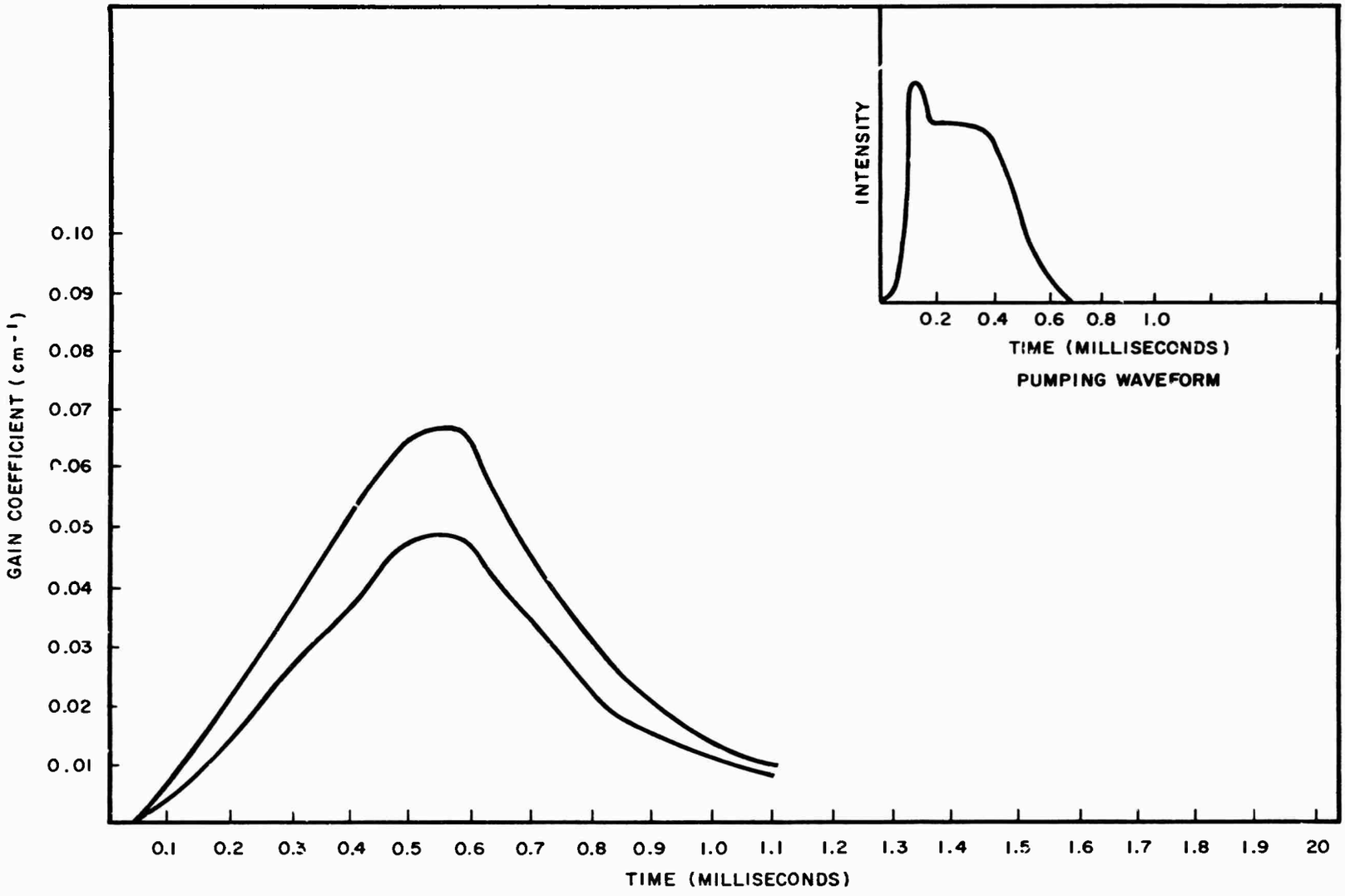

Fig. 4.6 TIME RESOLVED GAIN 440 MICROSECOND PUMP PULSE

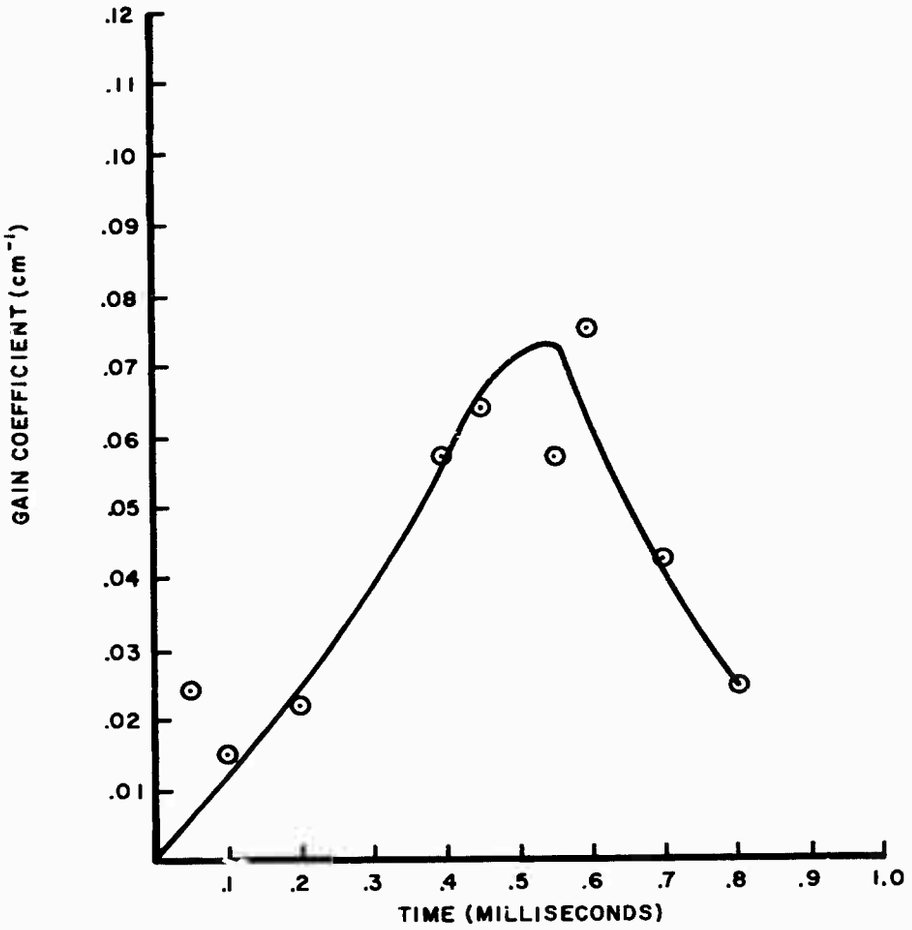

Fig. 4.7 TIME RESOLVED GAIN YAG LASER OSCILLATOR: INPUT PULSE
440 joules
440 microseconds

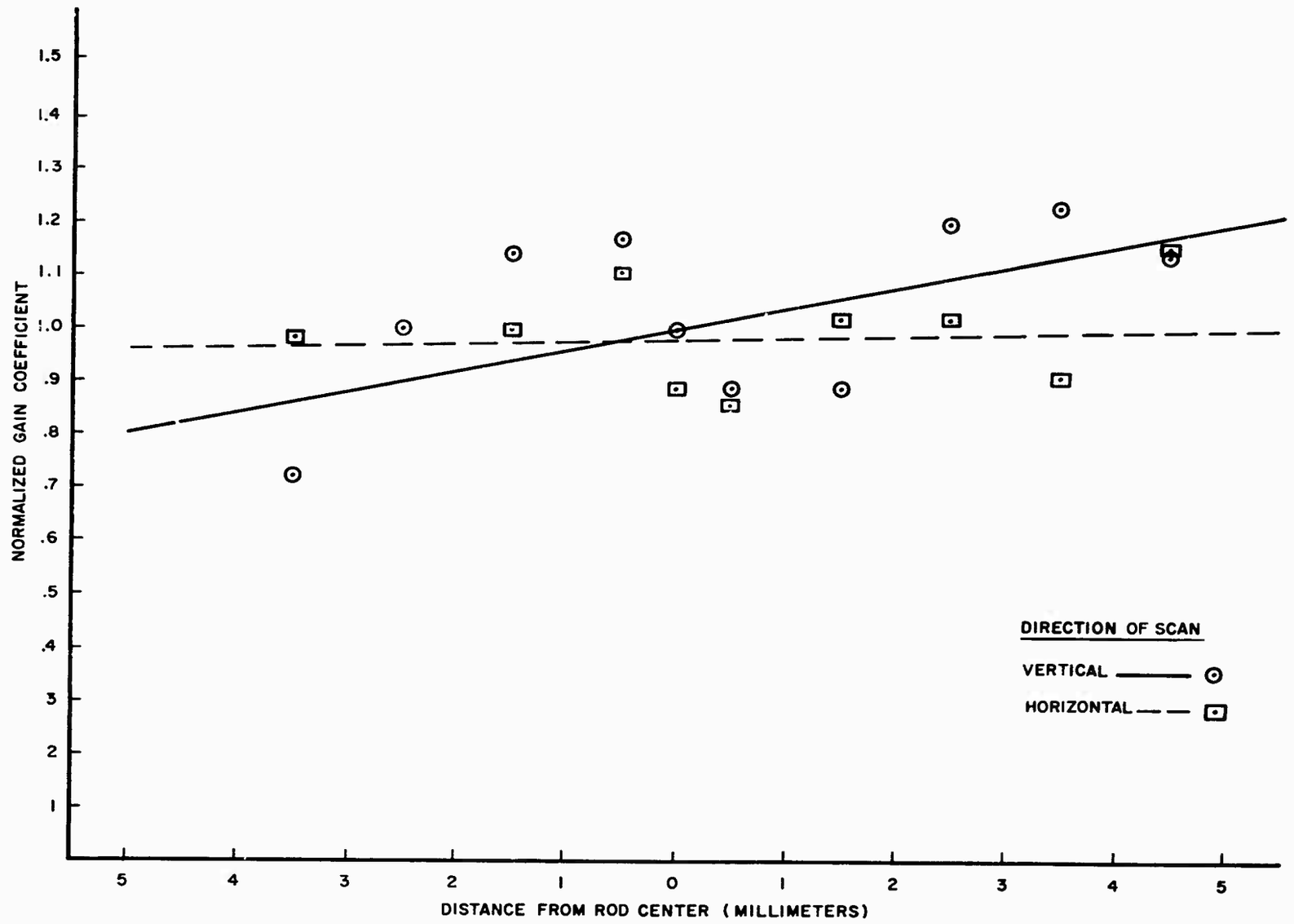

Fig. 4.8 GAIN DISTRIBUTION ACROSS THE FACE OF A 1 cm DIAMETER ROD

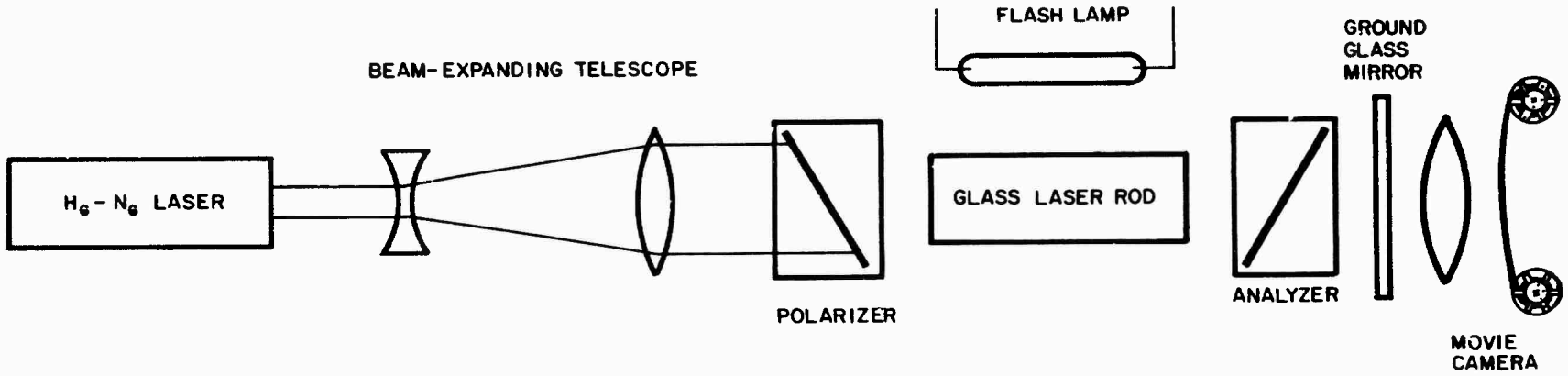

Fig. 5.1 APPARATUS FOR BIREFRINGENCE MEASUREMENTS

t < 0
(a)

t = .1 SEC
(b)

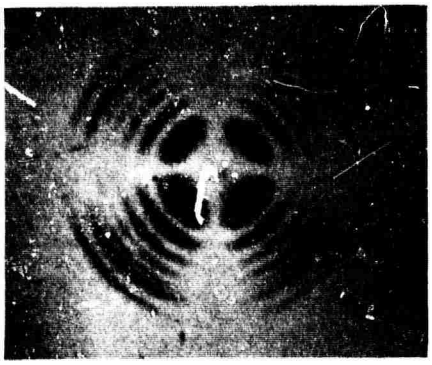

t = 2.4 SEC
(c)

t = 3.3 SEC
(d)

t = 8.7 SEC
(e)

t = 9.5 SEC
(f)

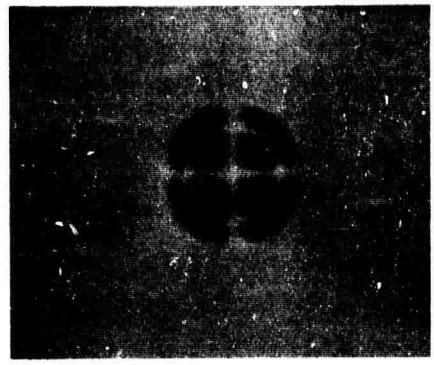

t = 13.1 SEC
(g)

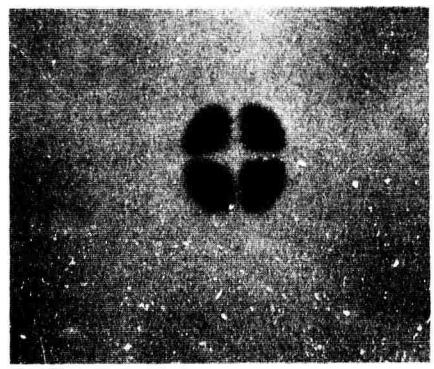

t = 18.6 SEC
(h)

FIG. 5.2 BIREFRINGENCE PATTERNS